International Journal of Biological Macromolecules 369 (2026) 152760

Contents lists available at ScienceDirect

International Journal of Biological Macromolecules

journal homepage: www.elsevier.com/locate/ijbiomac

Multi-spectroscopic and *in silico* approaches reveal the α-amylase and α-glucosidase inhibitory mechanism of anacardic acids and their effects on advanced glycation end products

Anna Elisabetta Maccarronello [a], Claudia Sciacca [a], Nunzio Cardullo [a], Luana Pulvirenti [b], Antonella Di Francesco [a], Vera Muccilli [a,*]

[a] Department of Chemical Sciences, University of Catania, V.le A. Doria 6, 95125, Catania, Italy
[b] CNR-ICB, Consiglio Nazionale delle Ricerche-Istituto di Chimica Biomolecolare, via Paolo Gaifami 18, Catania, 95126, Italy

ARTICLE INFO

Keywords:
Salicylic acid derivatives
α-Glucosidase
α-Amylase
Diabetes
Protein glycation
Human serum albumin

ABSTRACT

Anacardic acids (AAs) are a class of alkyl phenols widely distributed in the *Anacardiaceae* family and known for their diverse biological properties. However, their potential against type 2 diabetes mellitus (T2DM) has never been thoroughly investigated. In this study, a fraction isolated from a *Pistacia vera* shell extract, enriched in AAs, exhibited potent inhibitory activity against α-amylase (α-Amy) and α-glucosidase (α-Glu). Pure (15:0)-AA and (17:1)-AA also acted as strong inhibitors of both enzymes, displaying IC_{50} values significantly lower than those of the marketed anti-diabetic drug acarbose. Kinetic and molecular docking analyses identified both AAs as competitive α-Amy and α-Glu inhibitors that interact with the catalytic sites *via* non-covalent interactions. Fluorescence measurements revealed dynamic quenching upon AA-enzyme binding, while FT-IR and dynamic light scattering analyses demonstrated AA-induced conformational rearrangements and increased size distribution.

Beyond their hypoglycaemic potential, (15:0)-AA and (17:1)-AA strongly inhibited the formation of pathogenic advanced glycation end products (AGEs). AAs efficiently reduced fluorescent AGE formation in three distinct glycation models and effectively protected human serum albumin (HSA) from glycation-induced structural alterations, including exposure of hydrophobic domains and amyloid aggregation. Notably, AAs retained substantial antiglycation activity after simulated gastrointestinal digestion.

Overall, this work provides the first detailed insights into the hypoglycemic and antiglycation properties of AAs, supporting their potential application as multifunctional natural agents for T2DM management.

1. Introduction

In recent years, the search for novel therapeutic agents from natural sources has intensified, supported by their high biocompatibility and favorable safety profile compared to synthetic drugs [1]. Anacardic acids (AAs), also known as ginkgolic acids, are a class of long-chain alkyl phenols that naturally occur in the *Anacardiaceae* family, notably in cashew (*Anacardium occidentale*) nut shell liquid (CNLS) and the root bark of *Ozoroa insignis* [2,3]. Other botanical sources of AAs include *Pistacia vera* L. [4–7], *Juglans regia* L. [8], *Syzygium samarangense* [9] and *Ginkgo biloba* L. [10]. Structurally, these compounds are characterized by a salicylic acid moiety substituted with a hydrophobic side chain of varying length and unsaturation.

Emerging evidence highlights AAs as promising candidates for the management of diverse pathological conditions associated to oxidative stress [11], including acute respiratory distress syndrome [12], bacterial

Abbreviations: AA, Anacardic acid; AG, aminoguanidine hydrochloride; AGEs, advanced glycation end products; Arg, arginine; α-Glu, α-Glucosidase from *Saccharomyces cerevisiae*; α-Amy, α-Porcine pancreatic amylase; CNSL, cashew nut shell liquids; CNP-α-G3, 2-chloro-4-nitrophenyl-α-maltotrioside; DLS, dynamic light scattering; FA, formic acid; FRU, fructose; FT-IR, Fourier-transform infrared; G-HSA, glycated human serum albumin; HSA, human serum albumin; MAE, microwave-assisted extraction; MGO, methylglyoxal; OD, optical density; T2DM, Type 2 diabetes mellitus; PDI, polydispersity index; PVS, *Pistacia vera* L. shells; PVS-E, *Pistacia vera* L. shell extract; *p*NP-α-G, *p*-nitrophenyl-α-D-glucopyranoside; Trp, tryptophan.

* Corresponding author.
E-mail address: vera.muccilli@unict.it (V. Muccilli).

https://doi.org/10.1016/j.ijbiomac.2026.152760
Received 17 July 2025; Received in revised form 18 May 2026; Accepted 26 May 2026
Available online 28 May 2026

and fungal infections [2,13], inflammation [13], and pain [14]. Additionally, AAs have been shown to strongly inhibit target proteins such as histone acetyltransferase [13], lipoxygenase 1 [15], xanthine oxidase [16], and tyrosinase [17]. Notably, AAs-rich extracts from *Pistacia vera* L. [4,5] and *Syzygium samarangense* [9] have recently been identified as α-glucosidase (α-Glu) inhibitors, suggesting that the therapeutic potential of AAs could be extended to metabolic disorders such as type 2 diabetes mellitus (T2DM).

T2DM is a widespread chronic disorder characterized by hyperglycemia [18]. The inhibition of carbohydrate-hydrolysing enzymes, namely α-amylase (α-Amy; EC 3.2.1.1) and α-glucosidase (α-Glu, EC 3.2.1.20) represents a key strategy to reduce postprandial blood glucose levels and counteract hyperglycemia [19]. Despite their efficacy, conventional α-Amy and α-Glu inhibitors, such as acarbose and miglitol, are frequently associated with adverse gastrointestinal effects, flu-like symptoms, and skin reactions [18], prompting the search for safer, natural alternatives. While AAs show promise, a comprehensive evaluation of their potential inhibitory effects on α-Amy is still lacking, with only preliminary data available on their α-Glu inhibitory activity [9,20].

Notably, remarkable α-Amy and α-Glu inhibitory properties were previously observed by our research group for a *Pistacia vera* L. shell extract (PVS-E) and related to its bioactive constituents, including AAs [5]. Consequently, the present work investigated the inhibitory potential of an AA-rich fraction obtained from PVS-E against α-Amy and α-Glu. Subsequently, the inhibitory mechanisms of two major AAs identified in the fraction, namely (C15:0)-AA and (C17:1)-AA (Fig. 1), were characterized to explore the possible correlation between the hypoglycaemic activity of AA-containing extracts and that of individual AAs. Furthermore, new insights uncovered the role of AAs in counteracting protein glycation.

In diabetic patients, prolonged hyperglycemia promotes glycation, a non-enzymatic reaction between reducing sugars and proteins, leading to the formation of advanced glycation end products (AGEs) [21]. AGEs, such as glycated haemoglobin (HbA1c), can functionally alter nucleic acids and proteins, contributing to T2DM-related complications, including retinopathy and nephropathy [21]. Herein, human serum albumin (HSA), one of the most abundant plasma proteins in the body [22], was employed as a model protein to evaluate the antiglycation potential of AAs. To this end, methylglyoxal (MGO), a dicarbonyl compound, and arginine (Arg), a key amino acid involved in non-enzymatic glycation, were employed as reactive precursors of AGEs. The influence of AAs on the structural stability and conformational changes of HSA, along with their dicarbonyl scavenging capacity, was thoroughly assessed using Fourier-transform infrared (FT-IR) and fluorescence spectroscopy. Finally, an *in vitro* simulated gastrointestinal digestion was carried out to evaluate whether AAs retain their antiglycation activity after digestion.

By integrating multi-spectroscopic techniques and *in silico* modeling, this work provides crucial insights into the anti-diabetic and antiglycation mechanisms of AAs, thereby supporting the potential application of such a class of alkyl phenols in T2DM management.

2. Materials and methods

2.1. Reagents

All chemicals were of analytical (or superior) grade, as received from commercial sources. 6-pentadecylsalicylic acid ((15:0)-AA; ≥95.0%), 6-[(10Z)-heptadecenyl]salicylic acid ((17:1)-AA; ≥95.0%), catechin (≥97.0%), gallic acid (97.5–102.5%), quercetin-3-*O*-glucoside (≥98%), acetonitrile (CH_3CN), formic acid (FA), methanol (MeOH), 96% ethanol (EtOH), α-Glu from *Saccharomyces cerevisiae* (EC 3.2.1.20, Type I, lyophilized powder, ≥10 units/mg protein), α-Amy from porcine pancreas (EC 3.2.1.1, Type VI-B, >5 units/mg solid), *p*-nitrophenyl-α-D-glucopyranoside (pNP-α-G), starch from potato, 3,5-dinitrosalicylic acid (DNS), and 2-chloro-4-nitrophenyl-α-maltotrioside (CNP-α-G3), fluorescein sodium salt, fatty acid free human serum albumin (HSA; ≥99%), MGO solution (40 wt% in H_2O), aminoguanidine hydrochloride (AG), D-(−)-fructose, 8-anilino-1-naphthalenesulfonic acid (ANS), thioflavin T (ThT), 2,4-dinitrophenyl hydrazine (DNPH), and trichloroacetic acid were purchased from Merck (Darmstadt, Germany). α-Glu and α-Amy inhibition assays and kinetic analyses were performed on 96-well microplates and the Synergy H1 microplate reader (BioTek, United States) was used. α-Amy from human saliva (Type IX-A, 1000–3000 U/mg protein), calcium chloride dihydrate ($CaCl_2 \cdot 2H_2O$), pepsin from porcine gastric mucosa (3200–4500 U/mg protein), pancreatin from porcine pancreas (4 × USP), and bovine bile (B3883) were employed for the simulated gastrointestinal digestion as purchased from Sigma-Aldrich (Steinheim, Germany). Milli-Q water was employed in all the experiments.

2.2. Extraction and separation of anacardic acids

Pistacia vera L. shells (PVS), obtained from the Green Pistachio of Bronte (Italian Protected Designation of Origin (PDO) product; CE: Reg. EU No. 21, January 12, 2010), were kindly supplied by a pistachio manufacturer in Bronte (Catania, Italy) in December 2021. The shells were threefold washed with distilled water, dried at 35 °C for 48 h, and milled to a particle size of less than 1 mm. Subsequently, PVS (5 g) were subjected to microwave-assisted extraction (MAE), according to a previously optimized methodology [5]. The extraction conditions were as follows: 20% aqueous ethanol, 1000 W, 135 s, and a liquid/powder ratio of 27 mL/g. After extraction, the supernatant was vacuum-filtered and dried under reduced pressure. The resulting extract (PVS-E; 13.7% w/w) was stored at −20 °C until further experiments.

To separate AAs from PVS-E, a Sep-Pak C-18 cartridge (Waters, Milford, MA, USA) was preconditioned with 10 mL of acidified CH_3CN/H_2O (65:35 v/v + 0.1% FA), followed by 10 mL of H_2O/CH_3CN solution (98:2 v/v + 0.1% FA). PVS-E (33 mg) was completely dissolved in 25 mL of H_2O/CH_3CN solution (98:2 v/v + 0.1% FA) and slowly loaded onto the cartridge, yielding fraction 1 (F1; 29.6 mg). The cartridge was then sequentially eluted with 20 mL of H_2O/CH_3CN solutions at different ratios: 90:10 v/v (fraction 2, F2; 4 mg), 70:30 v/v (fraction 3, F3; 2.9 mg), 50:50 v/v, and 5:95 v/v. Based on their chromatographic profile, the last two eluates were combined to obtain fraction 4 (F4; 3.2 mg). All collected fractions (F1–F4) were dried and stored at +4 °C for further analyses. The recovery yields were 89.7% (F1), 12.1% (F2), 8.8% (F3), and 9.7% (F4), respectively.

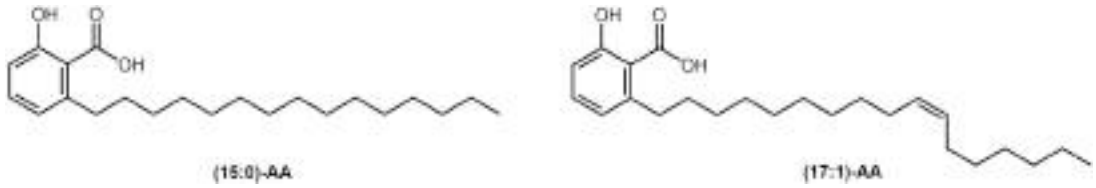

Fig. 1. 2D structures of (15:0)-AA and (17:1)-AA.

2.3. HPLC/ESI-MS/MS analysis of fractions obtained from Pistacia vera L. shell extract

Fractions (F1 – F4) obtained from PVS-E were analysed using an ion trap mass spectrometer equipped with an ESI ion source (LTQ, Thermo Fischer Scientific, San Jose, CA, USA) and coupled online with an LC pump (DionexUltimate 3000, Thermo Fischer Scientific, San Jose, CA, USA), according to a previously reported method [5]. All fractions (F1 – F4) were dissolved at a concentration of 1 mg/mL in a MeOH/H_2O mixture (50:50 *v*/v). Then, 20 μL of each sample were loaded into a Waters Symmetry RP-C18 column (150 mm × 1 mm i.d., 100 Å, 3.5 μm) maintained at 25 °C. Data acquisition and analyses were performed using Xcalibur *v*. 1.3 Software (Thermo Fischer Scientific, San Jose, CA, USA). The resulting total ion current (TIC) chromatograms are shown in Fig. S1A—D.

Quercetin 3-*O*-glucoside, (15:0)-AA, and (17:1)-AA were identified using commercial standards. The remaining compounds, for which standards were not available, were identified based on their retention time, chemical formulas, $[M-H]^-$ *m/z* values, and diagnostic MS/MS fragmentation patterns, as well as by comparison with MS data reported in the literature. Quantification was performed using external standard calibration curves (Fig. S2A—D) of gallic acid (Fig. S2A), quercetin 3-*O*-glucoside (Fig. S2B), (15:0)-AA (Fig. S2C), and (17:1)-AA (Fig. S2D). Semi-quantification of both gallic acid derivatives (GAs) and phenolic acids was carried out using gallic acid. Semi-quantification of flavonoids was achieved using quercetin-3-*O*-glucoside, while fatty acids (FAs) and AAs were quantified using (15:0)-AA. Results were expressed as mg of compound per g of dry weight (mg/g DW) ± standard deviation (SD).

2.4. α-Amylase and α-glucosidase inhibitory mechanism

2.4.1. In vitro α–glucosidase and α–amylase inhibition assays

The inhibitory effects of AA-rich fractions and pure AAs towards α-Amy and α-Glu was evaluated according to previous methods [5,23], as detailed in Supporting Material. AA-rich fractions were dissolved in a MeOH/H_2O mixture (50:50 v/v) at 1 mg/mL. Pure (15:0)-AA and (17:1)-AA were dissolved in methanol at 20 μM. Acarbose (3.1 mM) was analysed as a positive control in both bioassays. For α-Glu inhibition assay, changes in optical density (OD) were measured in quadruplicate at 405 nm. For α-Amy inhibition assay, OD measurements were acquired in quadruplicate at 540 nm. Inhibition percentages were calculated by Eq. (1), whereas the concentration required to inhibit 50% of α-Glu/α-Amy activity (IC_{50}) was determined by regression analysis and expressed in μg/mL and μM ± SD.

$$\text{Inhibition}\ (\%) = \frac{OD_{control} - OD_{sample}}{OD_{control}} \times 100 \tag{1}$$

2.4.2. Kinetic of α–glucosidase and α–amylase inhibition

The mode of α-Glu and α-Amy inhibition was spectrophotometrically determined by kinetic analysis, performed according to previously reported methods [1,23], as detailed in the Supporting Material. The Lineweaver–Burk equation, written in its double reciprocal form (Eq. (2)), was used to determine a competitive inhibition mechanism.

$$\frac{1}{v} = \frac{K_m\left(1 + \frac{I}{K_i}\right)}{v_{max}} \times \frac{1}{S} + \frac{1}{v_{max}} \tag{2}$$

Furthermore, the competitive inhibition constants (K_i) were determined in triplicate by secondary plots of the slope *versus* inhibitor concentration, as reported in Eq. 3 [24,25], where v and v_{max} are the initial rate of the enzymatic reaction and the maximal velocity, respectively, in the absence and presence of tested AAs; K_m and K_i are the Michaelis-Menten and the competitive inhibition constant, respectively; [*S*] and [*I*] are the concentrations of substrate (pNP-α-G) and inhibitor, respectively.

$$\text{Slope} = \frac{K_m}{V_{max}} + \frac{K_m[I]}{V_{max}K_i} \tag{3}$$

2.4.3. Molecular docking studies

The .sdf files of acarbose, (15:0)-AA and (17:1)-AA were downloaded from Pubchem (https://pubchem.ncbi.nlm.nih.gov/, ID cod respectively: 41774, 167551 and 5,469,634). The 3D models were geometrically minimized with optimized potential liquid simulation (OPLS3) force fields [26] considering the protonation state at pH of 7.0 ± 1 and processed using LigPrep interfaced with Maestro (13.7.125, MMshare Version 6.3.125) of Schröedinger suite [27]. The 3D structure of α-Amy (PDB ID: 1OSE) was downloaded from Protein Data Bank [28], whereas the 3D protein model of α-Glu was downloaded from AlphaFold Protein structure Database (https://alphafold.ebi.ac.uk/, PDB code: AF-P53341-F1-model_v4) [29]. The putative binding site of α-Glu was identified through the SiteMap software, which allowed the generation of a ranking of five possible druggable binding pockets based on the site score output. Hence, the best-one was used to obtain the following coordinates by Grid generation experiment: 14.61 (x), 2.13 (y), 1.91 (z), 10 × 10 × 10 as innerbox, and 36.76 × 36.76 × 36.76 as outerbox. The grid box of α-Amy was constructed by selecting in the Receptor Grid Generation tab, the co-crystallized inhibitor (acarbose) to specify the protein region suitable as binding site. In this way, the protein grid box was calculated, with the grid centre set at 35.61 (x), 37.36 (y) and −1.35 (z), using 20 × 20 × 20 as innerbox, and 40.80 × 40.80 × 40.80 as outerbox for α-Amy. Glide Ligand Docking interfaced with Maestro (Version 13) was employed for docking data analysis and the acquisition of 3D models. In the docking calculation, ligands were treated as flexible, while enzymes were treated as rigid and run in an OSX Ventura (13.2) environment.

2.4.4. Fluorescence spectra measurements

The interaction of (15:0)-AA and (17:1)-AA with α-Amy and α-Glu was investigated by quenching experiments, according to the procedure of Sciacca et al., with slight modifications detailed in the Supporting Material [1]. The fluorescence spectra of α-Amy and α-Glu were recorded on an Agilent Cary Eclipse fluorescence spectrophotometer (Milan, Italy) in the range 300–500 nm, setting the excitation wavelength (λ_{ex}) at 295 nm. All the measurements were performed by setting both excitation and emission slits at 10 nm, with a scan speed of 500 nm/min. Enzyme solutions (0.5 μM) were titrated with (15:0)-AA or (17:1)-AA (0–3.9 μM). All solutions were mixed and kept at specific temperatures (25, 30, and 37 °C) for 2 min before measurement. Fluorescence measurements were analysed according to the Stern–Volmer Eq. (4) [24]:

$$\frac{F_0}{F} = 1 + K_{SV}[Q] = 1 + K_q\tau_0[Q] \tag{4}$$

where F_0 and F are the maximum fluorescence intensity of the free enzyme (α-Amy or α-Glu) and the maximum fluorescence intensity of the protein-inhibitor complex, respectively; [*Q*] represents the concentrations of AAs; τ_0 is the average lifetime of the fluorophore in the absence of AAs, accounting for 10^{-8} *s* for both enzymes [24]; K_{SV} and K_q represent the quenching constant and the quenching rate constant, respectively. Therefore, the apparent binding constant (K_a) and the number of binding sites (*n*) were calculated using the following double-log Stern–Volmer Eq. (5) [23]:

$$\log\frac{F_0 - F}{F} = \log K_a + n\log[Q] \tag{5}$$

In addition, the fluorescence intensities were corrected for absorption of the excitation light and reabsorption of the emitted light to reduce the inner filter effect (IFE) according to Eq. (6) [30]:

$$F_{cor} = F_{obs}10^{(A_0 + A_{em})/2} \tag{6}$$

where F_{cor} and F_{obs} are the fluorescence intensities corrected and observed, respectively; and A_0 and A_{em} are the UV absorption values of the protein and ligands at the excitation and emission wavelengths, respectively [30]. The UV–Vis spectra of the two enzymes and AAs were recorded in the range of 200–700 nm using an Agilent Cary 60 UV–Vis spectrophotometer (Agilent Technologies Inc., Milan, Italy) in a 1.0 cm quartz cuvette at room temperature (Fig. S3A—B).

2.4.5. Fourier transform infrared (FT-IR) spectroscopy

The FT-IR spectra of α-Glu (0.8 μM) and α-Amy (6.9 μM) in 0.1 M phosphate buffer containing 0.1 M NaCl, pH 6.8, and their respective mixtures with AAs, as well as those of HSA and its glycated form with and without AAs, were acquired using a PerkinElmer SpectrumOne FT-IR spectrometer fitted with an ATR module. According to a previous method [31], spectra were recorded in the range of 4500–450 cm^{-1}, with a resolution of 4 cm^{-1} and 60 scans per measurement. In the FT-IR experiments conducted on α-Glu and α-Amy, 2 mM stock solutions of (15:0)-AA and (17:1)-AA were used. For the FT-IR measurements of HSA glycated complexes, both AAs were tested at 0.4 mM. The spectral region 1700–1600 cm^{-1} was carefully analysed to investigate the enzyme–AA interactions and glycated HSA-AAs interactions, respectively. All FT- IR data were obtained as the average of three replicates.

2.4.6. Dynamic light scattering (DLS) measurements

DLS measurements were performed using a Zetasizer Pro instrument (Malvern Panalytical Ltd., United Kingdom) to study the variation in the size distribution (d, nm) of α-Amy and α-Glu in the presence of AAs. Following a previous method [32], data were reported as size distribution (nm). In the experiments, each enzyme (2 mg/mL in 50 mM phosphate buffer, pH 6.8) was mixed with 20 μL of MeOH (reference) or with AAs (2.8 mM). The mixtures were incubated at 37 °C for 15 min and then centrifuged at 5000 rpm for 10 min. Hence, the resulting solutions were filtered through a 0.45 μm PTFE membrane and employed for measurements. Samples were acquired in triplicate and processed in three 5 min runs.

2.5. In vitro inhibitory effect of anacardic acids (AAs) on advanced glycation end products (AGEs)

2.5.1. Antiglycation activity assay

The inhibitory efficacy of (15:0)-AA and (17:1)-AA towards AGEs formation was tested by three different non-enzymatic protein glycation models, namely HSA/FRU, HSA/MGO, and Arg/MGO, respectively, following the method described by Wang et al., [33] with slight modifications [34], as detailed in the Supporting Material. AG and catechin were employed as positive controls. Blank solutions were obtained by replacing samples/controls with the same amount of 50 mM sodium phosphate buffer pH 7.4, containing 0.02% sodium azide. Briefly, AAs, AG and catechin were dissolved in a MeOH/H_2O mixture (50:50 *v*/v) and serially diluted from 2 to 0.15 mg/mL in sodium phosphate buffer (50 mM, pH 7.4, with 0.02% sodium azide) for IC_{50} determination. The degree of protein glycosylation was assessed in triplicate by monitoring the changes in AGEs fluorescence emission within 340–420 nm. Hence, AGEs inhibition percentages (%) were calculated using the following Eq. (7):

$$\text{Inhibition of fluorescent AGEs (\%)} = \frac{F_0 - F}{F_0} \times 100 \quad (7)$$

where F and F_0 represent the fluorescence intensity with and without inhibitors/controls, respectively. IC_{50} values were calculated by regression analysis and expressed in μg/mL ± SD.

2.5.2. Methylglyoxal-induced structural changes of human serum albumin (HSA)

The glycosylation reaction of HSA was performed using MGO, according to previously reported methods [35,36], with slight modifications. Glycated HSA (G-HSA) was prepared under aseptic conditions in 50 mM phosphate buffer (pH 7.4, 0.02% sodium azide) by incubating HSA (10 mg/mL) with MGO (10 mM) in the absence and presence of different concentrations (0.05–0.4 mM) of tested AAs (1:1:1 *v*/v). AG (0.4 mM) was treated as a sample and used as a positive control. Protein mixtures were pre-incubated for 10 min at 37 °C before the addition of 10 mM MGO and then kept for 4 days at 37 °C in the dark. HSA alone (hereafter referred to as native HSA) was used as a control. All protein mixtures were prepared in triplicate.

After the incubation period, changes in the fluorescence emission signals of all mixtures were monitored at 440 nm upon excitation at 370 nm using a Varioskan Flash multimode reader (Thermo Fisher Scientific, Inc. Waltham, MA, USA). Protein mixtures were stored at −20 °C until further experiments.

2.5.3. ANS fluorescence measurements

The exposure of hydrophobic domains in native, G-HSA, and G-HSA treated with AAs was assessed using ANS. This hydrophobic fluorescent probe is widely used for the characterization of protein binding sites [37]. According to a previous method [35], 5 μL of 5 mM ANS solution were added to 2995 μL of each protein sample and incubated for 5 min at room temperature in the dark before fluorescence measurements. Emission spectra were recorded in the range of 400–600 nm with excitation at 385 nm. All the measurements were carried out in triplicate, and their average was used for data elaboration.

2.5.4. ThT fluorescence assay

In this study, ThT fluorescence was used to evaluate amyloid formation in G-HSA and the protective role of AAs against glycation-induced aggregation and fibrillation. Native HSA was tested as a control. According to a previous method [35], 20 μL of G-HSA or HSA/AA mixtures were combined with 980 μL of ThT solution (10 μM ThT in phosphate buffer, pH 7.4). Fluorescence intensity was recorded at 485 nm with excitation at 430 nm. The degree of inhibition (%) was calculated using Eq. (8):

$$\%\text{inhibition} = \frac{F_g - F_t}{F_g - F_n} \times 100 \quad (8)$$

where F_g, F_t, and F_n represent the fluorescence intensities of glycated, treated, and native HSA samples, respectively.

2.5.5. Determination of dicarbonyl compounds by DNPH assay

The ability of AAs to scavenge reactive dicarbonyl compounds was evaluated following a well-established procedure [38], with minor changes [39]. G-HSA and G-HSA treated with 0.1 mM (15:0)-AA and (17:1)-AA (200 μL) were mixed with 400 μL of a 7 mM DNPH solution prepared in 2 M HCl and incubated for 1 h at room temperature. Subsequently, 500 μL of 4% (w/v) trichloroacetic acid was added to precipitate the proteins. Each mixture was centrifuged at 14,000 ×*g* for 5 min, and the resulting supernatant was discarded. The pellet was washed with a 1:1 v/v ethanol/ethyl acetate solution and centrifuged. This washing step was repeated four times to remove excess DNPH. The final pellet was dissolved in 0.6 mL of 6 M guanidinium hydrochloride (prepared in 20 mM phosphate buffer, pH 2.3). Samples were frozen overnight at −20 °C to ensure complete dissolution of hydrazones. Subsequently, absorbance was measured at 379 nm. Native HSA was tested as a control. Results were expressed as moles of dicarbonyl per mole of HSA, calculated in triplicate using a molar absorption coefficient of $\varepsilon_{379\ nm} = 22{,}000\ M^{-1}\ cm^{-1}$ [38].

2.5.6. In vitro simulated gastrointestinal digestion

AAs were subjected to the *in vitro* simulated digestion method proposed by Minekus et al. [40], with minor modifications [41]. AAs were dissolved in ethanol at 3 mg/mL and mixed at a 1:1 v/v ratio with a

simulated salivary fluid (SSF) containing salivary α-amylase (75 U/mL), adjusted to pH 7 with 0.3 M $CaCl_2{\cdot}2H_2O$. Each mixture was incubated at 37 °C for 2 min. Subsequently, 0.2 mL of the oral digest was collected in duplicate and replaced with an equal volume of SSF. For the gastric stage, simulated gastric fluid (SGF; pH 3) containing porcine pepsin (2000 U/mL) and 0.3 M $CaCl_2{\cdot}2H_2O$ was added to the previous mixture and incubated at 37 °C. After 2 h, 0.2 mL of the gastric digest was collected in duplicate and replaced with an equal volume of SGF. The intestinal phase was initiated by adding a simulated intestinal fluid (SIF) containing pancreatin (100 U/mL) and bile salts (10 mM) at pH 7 to the gastric digest. Each mixture was incubated for 2 h under agitation at 37 °C. Hence, 1 mL of the intestinal digest was collected in duplicate. Blank samples were prepared by replacing the AAs solution with ethanol. All digested samples were centrifuged at 12,000 rpm for 5 min at 4 °C, and the resulting supernatants were collected and stored at −20 °C until the *in vitro* antiglycation assay.

The same *in vitro* digestion protocol was also applied to G-HSA (control) and G-HSA treated with 0.4 mM AAs. Subsequently, the digested samples were used for direct fluorescence AGE determination (λ_{ex} = 370 nm; λ_{em} = 440 nm).

2.5.7. Antiglycation effect of anacardic acids (AAs) after in vitro digestion

The antiglycation activity of digested AAs was assessed using the HSA/MGO glycation model, as detailed in Section 2.5.2. Results were obtained in triplicate and expressed as the inhibition rate of AGEs formation, calculated using Eq. (9) [41]:

$$\text{Inhibition rate}\ (\%) = \frac{F_{\text{control}} - F_{\text{digest}}}{F_{\text{control}} - F_{\text{blank}}} \times 100 \quad (9)$$

where F_{digest} represents the fluorescence intensity of digested AAs in each digestive phase, F_{blank} is the fluorescence intensity of the digestive fluid with distilled water, and F_{control} is the fluorescence intensity of the digestive fluid without AAs.

2.6. Statistical analysis

To investigate statistical significance, one-way ANOVA analyses were performed using OriginPro 2023 software (Northampton, Massachusetts, USA), followed by Tukey's pairwise comparison test ($p < 0.05$).

3. Results and discussion

3.1. Phytochemical profile of fractions obtained from Pistacia vera L. shell extract

According to our previous work [5], PVS-E constituents comprise five classes of compounds, namely organic acids (1,2), gallic acid derivatives, including hydrolysable tannins (3–5, 7, 9, 14, 19, 23, 24), flavonoids (6, 8, 10–13, 15–17, 20, 21, 25, 26, 30), fatty acids (22, 27–29, 31–39, 44, 45) and AAs (41–43, 46–52) [5]. In this study, PVS-E was fractionated on a Sep-Pak C18 cartridge, with stepwise elution under acidic conditions employing CH_3CN/H_2O to obtain a fraction enriched in AAs. The resulting fractions (F1 – F4) were qualitatively and quantitatively characterized by HPLC/ESI-MS/MS (Table S1). Representative Total Ion Current (TIC) chromatograms obtained in negative ionization mode for fractions F1 – F4 are shown in Fig. S1A—D.

Fraction F1 was characterized by the presence of an intense peak at the beginning of the TIC chromatogram (t_r = 1.7–3.5 min, Fig. S1), consisting of co-eluting organic acids, namely malic (1) and quinic (2) acids, which were quantified together (88.61 mg/g DW).

Fractions F2 – F3 were characterized by the presence of gallic acid derivatives (digallic acid, 4; ethyl gallate, 9; pentagalloyl glucose isomer, 19; digalloyl hexose, 23; gallic acid derivative, 24), luteic acid (18), and flavonoids, including aspalathin (6), taxifolin (15), quercetin (25), kaempferol (26), and dihydrokaempferol (30), as well as derivatives of quercetin (quercetin galloyl hexoside isomer, 13; quercetin hexoside, 16; quercetin monoglucuronide, 17; quercetin pentoside, 20; quercetin-*O*-hexosedeoxyhexoside, 21) and myricetin (myricetin galloyl hexoside, 8; myricetin hexuronide, 10; myricetin rhamnohexoside, 11; myricetin hexoside, 12). Specifically, fraction F2 was distinguished by its high content of ethyl gallate (76.90 mg/g DW), quercetin galloyl hexoside isomer (0.38 mg/g DW), and luteic acid (4.31 mg/g DW), whereas flavonoids were mostly concentrated in F3. Although AAs were detected in fractions F1 – F3, the highest concentrations were found in F4 (Table 1; Table S1).

F4 exhibited a markedly different composition, with a clear enrichment in AAs. Its TIC chromatogram (Fig. S1D) was dominated by intense peaks eluting at high retention times (t_r = 60–66 min), corresponding to less polar compounds, including fatty acids and AAs. The total content of AAs in F4 reached 24.86 mg/g DW, which was significantly ($p < 0.05$) higher compared with the amount detected in F1 – F3 (Table 1). F4 included 85.69% of the total AAs quantified in PVS-E, reflecting the high efficiency of the applied fractionation process in concentrating such compounds into a single fraction. Specifically, (14:1)-AA was detected among the most abundant AAs (5.50 mg/g DW), followed by (13:1)-AA (3.02 mg/g DW), (13:3)-AA (2.59 mg/g DW), (15:0)-AA (2.46 mg/g DW), and (17:1)-AA (2.73 mg/g DW). Additionally, (13:0)-AA, (15:1)-AA, and (17:3)-AAs were consistently found in F4 (Table S1), highlighting fractionation on Sep-Pak C18 as an effective strategy for the recovery of AAs from PVS-E.

3.2. Hypoglycaemic effect of anacardic acid-rich fractions

α-Amy and α-Glu are key hydrolytic enzymes involved in the breakdown of carbohydrates during digestion. α-Amy, secreted in its active form by salivary glands, begins starch digestion in the oral cavity, hydrolysing it into maltose and dextrins. This process continues in the duodenum through the action of pancreatic α-Amy. Afterward, α-Glu hydrolyses glycosidic bonds (α-1,4 and/or α-1,6), breaking down the residual polysaccharides produced by α-Amy into absorbable monosaccharides, mainly glucose [43]. Accordingly, α-Amy and α-Glu inhibition represent a strategy to manage postprandial increases in blood glucose levels and insulin response [43,44].

Recent studies have highlighted the α-Glu inhibitory potential of AAs-containing extracts from *Pistacia vera* hulls [4] and *Syzygium samarangense* leaves [9]. Additionally, a recent investigation has revealed an appreciable inhibitory capability towards both α-Amy and α-Glu by an extract obtained from pistachio hard shells (PVS-E) [5]. The extract's hypoglycaemic properties have been related to its bioactive constituents, including AAs. Nevertheless, a direct correlation between the activity of AAs-containing extracts and that of individual AAs remained unestablished.

In the present work, fractions F1 – F4 obtained from PVS-E were

Table 1
Total contents of organic acids, gallic acid derivatives, flavonoids, fatty acids, and anacardic acids (AAs) determined by HPLC-ESI-MS/MS analysis in fractions F1 – F4 obtained from *Pistacia vera* L. shell extract (PVS-E).

	F1	F2	F3	F4
Total organic acids	88.61 ± 1.46^{a}	4.31 ± 0.12^{b}	–	–
Total gallic acid derivatives	–	77.28 ± 1.32^{a}	0.32 ± 0.03^{b}	–
Total flavonoids	–	7.82 ± 0.23^{a}	1.35 ± 0.14^{b}	–
Total fatty acids	3.92 ± 0.81^{b}	2.04 ± 0.11^{c}	3.58 ± 0.29^{b}	9.44 ± 1.02^{a}
Total anacardic acids (AAs)	3.37 ± 0.59^{b}	1.19 ± 0.37^{d}	2.34 ± 0.43^{c}	24.86 ± 0.62^{a}

Results are expressed in mg/g DW and reported as means ± SD. Different letters in the same row indicate statistically significant differences ($p < 0.05$, Tukey's test).

screened for their inhibitory effects on α-Amy and α-Glu, together with two pure AAs identified in the fractions, according to a well-established procedure [1,5]. The results, expressed as IC_{50} values (μg/mL), are summarized in Table 2.

Considering that lower IC_{50} values reflect higher inhibitory effectiveness, F4, which contained the highest concentration of AAs (Table 1), exhibited the strongest hypoglycaemic activity towards both target enzymes, being only 9.7% of the total eluate. Specifically, F4 displayed an α-Amy inhibitory activity of 3.18 μg/mL, which was significantly ($p < 0.05$) stronger than that observed for fractions F1–F3 and the anti-diabetic drug acarbose (7.68 μg/mL). Similarly, F4 showed a markedly higher α-Glu inhibitory effect (5.14 μg/mL) than F1–F3, PVS-E (41.07 μg/mL), and acarbose (88.25 μg/mL).

Herein, pure AAs were tested as new natural inhibitors of both α-Glu and α-Amy. The potential administration of AAs to diabetic patients was first considered by Toyomizu et al. [20], who reported preliminary data on the α-Glu inhibitory activity of some 6-alkylsalicylic acids isolated from CNLS (*Anarcardium occidentale*), while no studies have been performed on the potential inhibitory behaviour of such alkyl phenols towards α-Amy. Pure (15:0)-AA and (17:1)-AA strongly inhibited α-Glu (13.21 μM and 9.42 μM, respectively), in line with previous findings on 6-alkylsalicylic acids and derivatives [9,20]. Tested AAs also showed a remarkable α-Amy inhibitory capacity (7.46 μM and 6.36 μM, respectively). Moreover, their activity towards both the enzymes was superior to that observed for acarbose (Table 2).

Worth noting, pure AAs showed α-Glu and α-Amy inhibitory activities comparable ($p > 0.05$) to those of F4, corroborating the hypothesis that they are key contributors to the observed hypoglycaemic effects. Consequently, this study aimed to elucidate fully, for the first time, the inhibitory behaviour of AAs towards both α-Amy and α-Glu, addressing the lack of a direct correlation between the hypoglycaemic activity displayed by AAs-containing extracts and that of individual AAs. To this end, (15:0)-AA and (17:1)-AA were subjected to computational, kinetic, and fluorescence analyses to evaluate their inhibition mechanism and binding affinities towards α-Amy and α-Glu. The results are discussed in the following.

3.3. Molecular modeling

In this investigation, molecular docking was employed to evaluate the binding affinity of tested (15:0)-AA (X) and (17:1)-AA (Y) towards α-Glu and α-Amy catalytic sites. The ligand-protein interactions are summarized in Tables 3 and 4. To validate the models, acarbose was employed as a positive control for both α-Glu and α-Amy.

Table 2
Hypoglycaemic effect of fractions obtained from *Pistacia vera* L. shell extract and pure anacardic acids (AAs) towards α–amylase (α–Amy) and α –glucosidase (α–Glu). Results are reported as mean ± SD ($n = 3$).

	Hypoglycaemic activity	
	α-Amy IC_{50}, μg/mL	α–Glu IC_{50}, μg/mL
PVS-E[#]	2.05 ± 0.84^{f}	41.07 ± 1.30^{c}
F1	32.36 ± 2.94^{b}	96.38 ± 1.88^{a}
F2	103.90 ± 4.45^{a}	24.73 ± 3.33^{d}
F3	20.54 ± 3.77^{c}	45.29 ± 1.80^{c}
F4	3.18 ± 0.31^{e}	5.14 ± 0.62^{e}
(15:0)-AA	2.59 ± 0.55^{e} (7.46 ± 0.49 μM)[*]	4.60 ± 0.16^{e} (13.21 ± 0.68 μM)[*]
(17:1)-AA	2.38 ± 0.43^{e} (6.36 ± 1.14 μM)[*]	3.53 ± 0.31^{f} (9.42 ± 0.83 μM)[*]
Acarbose	7.68 ± 0.73^{d}	88.25 ± 7.81^{b}

Different letters in the same column indicate statistically significant differences (Tukey's test, $p < 0.05$).

[#] Data previously reported, stated in the table only for comparison purposes [5].

[*] Values in brackets correspond to IC_{50} values expressed in μM.

Table 3
Binding energy (ΔG_{bind}), molecular interactions and residues interacting with (15:0)-AA and (17:1)-AA within the α-glucosidase (α-Glu) catalytic site.

Ligands	Glide calcd ΔG_{bind}	Interacting residues	Interaction type	Ligand functional group	Distance (Å)
(15:0)-AA	−4.40 kcal/mol				
		Lys155	H-bond	C=O (carboxyl group)	1.95
		Lys155	salt bridge	OH (carboxyl group)	3.34
		Hie239[a]	π – π stacking	aromatic ring	5.19
		Hie239[a]	aromatic H bond	C=O (carboxyl group)	3.15
		Phe311	aromatic H bond	OH (carboxyl group)	3.62
(17:1)-AA	−4.35 kcal/mol				
		Hip279[a]	Salt bridge	OH (carboxyl group)	2.81
		Hip279[a]	H-bond	OH (−carboxyl group)	2.09
		Hip279[a]	aromatic H bond	C=O (carboxyl group)	3.25
Acarbose	−7.09 kcal/mol[b]	–	–	–	–

[a] Histidine residues are labelled according to their protonation state: HIE (ε-protonated) and HIP (doubly protonated, positively charged).

[b] Result previously reported by our research group, stated in the table only for comparison purposes [1].

Fig. S4 shows the molecular surface models of α-Glu (cherry wood) and α-Amy (faded red orange) with the natural ligands overlapping within the binding sites and suggests a good compatibility in terms of shape and size for the hydrophobic pocket. Binding energy ranged from −4.62 to −4.35 kcal/mol for α-Glu and from −5.04 to −4.66 kcal/mol for α-Amy. Although their docking scores are less favorable than that of acarbose, this difference can be attributed to their simpler chemical structures and the lower number of polar functional groups, which limits the formation of hydrogen bonds compared to acarbose. Nevertheless, the hydrophobic alkyl chain of anacardic acids contributes to stabilizing interactions within the binding pocket, supporting their effective binding. Visual inspection of docking poses confirmed consistent accommodation of both ligands within the catalytic sites.

In general, the two ligands can interact by forming non-covalent interactions through the aromatic portion of their molecular structure, which includes a phenolic OH substituent at C-2 and an acidic group at C-1. Further, the aliphatic chain appears to stabilize the pose due to hydrophobic interactions. For α-Glu, (15:0)-AA interacts with key residues such as Lys155, Hie239 and Phe311through hydrogen bonds, salt bridges, and π – π stacking interactions, resulting in a binding energy of −4.62 kcal/mol (Table 3, Fig. 2A).

Similarly, (17:1)-AA interacts within the same binding region (Fig. 2A), mainly involving Hip279, with a comparable binding energy (−4.35 kcal/mol). These findings are consistent with the *in vitro* results (Table 2), which showed significant inhibitory activity for both compounds.

Table 4
Binding energy (ΔG_{bind}), molecular interactions and residues interacting with (15:0)-AA and (17:1)-AA within the α-amylase (α-Amy) catalytic site.

Ligands	Glide calcd ΔG_{bind}	Interacting residues	Interaction type	Ligand functional group	Distance (Å)
(15:0)-AA	−4.66 kcal/mol				
		Thr52	H-bond	OH (carboxyl group)	2.32
		Asn53	H-bond	OH (−carboxyl group)	1.95
		Val50	H-bond	OH (carboxyl group)	2.33
(17:1)-AA	−5.04 kcal/mol				
		Thr52	H-bond	OH (carboxyl group)	2.35
		Asn53	H-bond	OH carboxyl group)	1.96
		Val50	H-bond	OH (carboxyl group)	2.33
Acarbose	−6.70 kcal/mol[a]	–	–	–	–

[a] Result previously reported by our research group, stated in the table only for comparison purposes [1].

The results are also promising in the case of α-Amy, for which ΔG values of −4.66 and −5.04 kcal/mol were obtained for (15:0)-AA and (17:1)-AA, respectively (Table 4). Both ligands are well accommodated within the hydrophobic cavity, with the alkyl chain deeply inserted and the aromatic head oriented towards the pocket entrance. In α-Amy, (15:0)-AA forms hydrogen bonds with Thr52, Asn53, and Val50, involving both the carboxyl and phenolic groups.

The same coordination type with α-Amy was observed for (17:1)-AA (teal), confirming the very similar inhibition values obtained from the *in vitro* biochemical assays (Table 2). Overall, the *in silico* analysis supported the ability of both AAs to interact with the catalytic sites of α-Glu and α-Amy, suggesting a potential competitive inhibition mechanism.

3.4. Kinetic of α-amylase and α-glucosidase inhibition

The inhibition mechanism of the tested AAs towards α-Amy and α-Glu was investigated by following a previously reported spectrophotometric approach [1,23]. Lineweaver-Burk plots of α-Amy and α-Glu inhibition in the presence of (15:0)-AA and (17:1)-AA are reported in Fig. 3A–B. Graphs were obtained by plotting the reciprocal of enzyme reaction rate (ν) against the reciprocal of the substrate concentration (CNP-α-G3 for α-Amy and NP-α-G for α-Glu). Specifically, each inhibitor was tested at five different concentrations, yielding five straight lines that intersected at a single point. Additionally, kinetic inhibitory constants (K_i) of (15:0)-AA and (17:1)-AA were estimated according to Eqs. (4)–(5) and are listed in Table 5. All the results were compared with previously published data on acarbose, which has been identified as a competitive inhibitor of both α-Amy and α-Glu [1,45].

According to Fig. 3A–B, both AAs act as competitive inhibitors, with the lines intersecting the *y*-axis in the first quadrant [24,44], thus supporting the molecular docking results. Competitive inhibitors bind to the enzyme active site, displacing the substrate in a concentration-dependent manner [46]. In this type of inhibition, the characteristic Michaelis-Menten kinetic show an increase in K_m, while V_{max} remains unchanged [45]. According to Fig. 3A, increasing concentrations of AAs did not affect the V_{max} value (0.01 μM min^{-1}) and increased the K_m values ((15:0)-AA: from 0.88 to 2.67 μM; (17:1)-AA: from 1.13 to 3.26 μM), supporting the finding that tested compounds competitively inhibit the α-Amy activity [45]. In addition, the secondary plots of the slope fitted linearly against the different inhibitor concentrations, indicating that AAs bind to α-Amy at the catalytic site [25,47].

Concerning α-Glu inhibition (Fig. 3B), K_m values of both AAs gradually increased ((15:0)-AA: from 6.33 to 11.9 μM; (17:1)-AA: from 2.67 to 7.25 μM), while the V_{max} value remained constant at 0.45 μM min^{-1}, corroborating the occurrence of a competitive inhibition mechanism [46], confirming the *in silico* outcomes. Moreover, as depicted in the insets of Fig. 3B, the secondary plots of slope *versus* inhibitor concentration showed a linear fit, confirming that the enzyme-inhibitor complex formation occurred *via* a competitive mechanism [24].

K_i values of tested AAs (Table 5) were consistent with their experimental IC_{50} values (Table 2), with (17:1)-AA being statistically ($p < 0.05$) more effective than (15:0)-AA towards both α-Amy and α-Glu.

3.5. Fluorescence quenching studies

The affinity of both (15:0)-AA and (17:1)-AA for α-Amy and α-Glu was investigated through fluorescence quenching experiments conducted at three different temperatures (25, 30, and 37 °C). Tryptophan (Trp) and tyrosine (Tyr) are the primary amino acids responsible for the intrinsic fluorescence of proteins [23]. When an enzyme interacts with a ligand, changes in the local microenvironment around Trp residues can lead to a reduction in the enzyme's intrinsic fluorescence intensity [48]. Figs. 4A–B and 5A–B present the fluorescence emission spectra of α-Glu and α-Amy, respectively, recorded before and after the addition of the tested AAs at an excitation wavelength of 295 nm. Both α-Glu and α-Amy exhibited a strong fluorescence emission peak at 330 nm, attributed to aromatic Trp and Tyr residues within their structures [1]. In comparison, AAs alone displayed a fluorescence peak at 410 nm under the same experimental conditions. Notably, the addition of increasing concentrations of tested AAs led to a progressive decrease in the fluorescence intensity of both the enzymes (Figs. 4–5A–B), indicating that AAs interact with the two enzymes, altering the environment around their Trp and Tyr residues.

Data from fluorescence measurements allowed us to elaborate the Stern-Volmer plots shown in Fig. 6A–B. A unique quenching mode was observed from the interaction of (15:0)-AA and (17:1)-AA with α-Amy and α-Glu, as evidenced by the linear fitting of the Stern-Volmer plots (Fig. 6A–B) [30]. Stern–Volmer quenching constant (K_{SV}) and apparent binding constant (K_a) were obtained by applying Eqs. (4) and (5) and are shown in Table 6.

In all experiments, an increase in temperature led to greater collisions and a consequent rise in K_{sv} values, suggesting that both AAs interact with each enzyme through a dynamic quenching mechanism [1,45]. Specifically, K_{sv} values of (15:0)-AA increased from 7.28 to 10.03 × 10^4 L/mol for α-Amy and from 11.54 to 14.50 × 10^4 L/mol for α-Glu. Analogously, K_{sv} values of (17:1)-AA increased from 6.44 to 10.40 × 10^4 L/mol for α-Amy and from 12.51 to 16.55 × 10^4 L/mol for α-Glu. K_{sv} values in the range of 10^4 indicate a strong binding affinity to both the enzymes [25]. According to Table 6, the number of binding sites (n) was close to 1 for both AAs, suggesting the formation of a one-to-one complex between each enzyme and the corresponding quencher [1,25]. Considering the resulting K_a values (Table 6), AAs exhibited similar affinity towards both enzymes, consistent with the outcomes of the *in vitro* and *in silico* studies.

3.6. Effect of anacardic acids (AAs) on the structure and size of α-glucosidase and α-amylase

3.6.1. FT-IR measurements

The conformational changes of α-Glu and α-Amy induced by the interaction with AAs were also investigated using FT-IR spectroscopy.

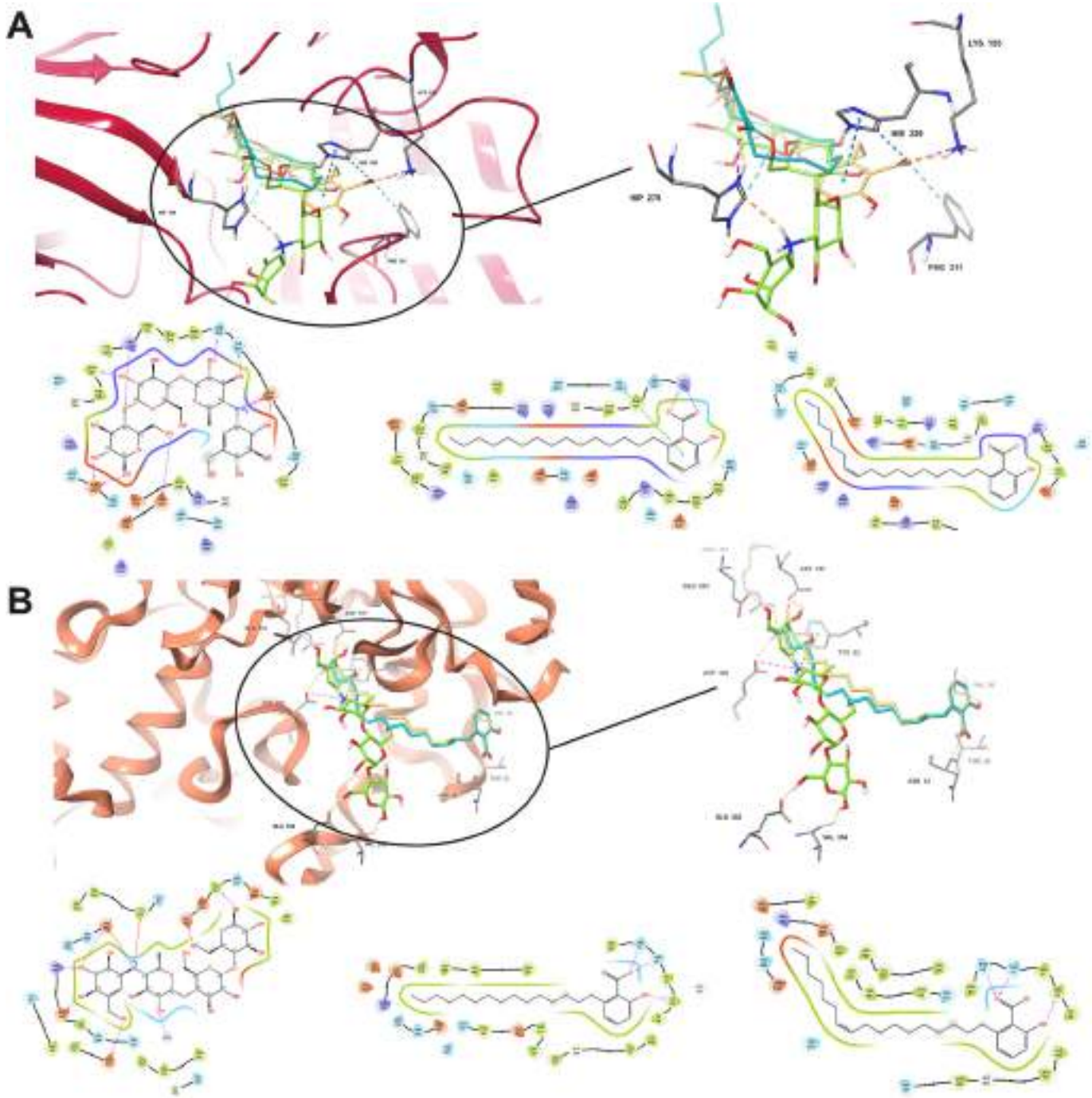

Fig. 2. A–B. (15:0)-AA (faded orange), (17:1)-AA (teal) and acarbose (green) into (A) α-Glu and (B) α-Amy binding sites, as well as their respective 2D interaction diagrams.

The amide bands of proteins typically appear in the 1700–1600 cm^{-1} region (C═O stretching, known as the amide I band) and 1600–1500 cm^{-1} region (C—N stretching and N—H bending, known as the amide II band) [49]. As the amide I band is more sensitive to variations in protein secondary structures than the amide II band, the 1700–1600 cm^{-1} region was analysed in depth to highlight the conformational changes and variations in the relative content of secondary structure elements resulting from the interaction of AAs with the two enzymes.

As shown in Fig. 7A–F, the amide I band peaks of free α-Glu (1679, 1663, 1647, 1631, and 1616 cm^{-1}) shifted to higher wavenumbers after the addition of (15:0)-AA and (17:1)-AA, suggesting interactions with C═O groups and rearrangement of the hydrogen bonding pattern [31]. The same trend was observed for free α-Amy and α-Amy-AA mixtures.

Curve-fitting analysis of the amide I region was used to determine the relative content of each secondary structure element in α-Glu and α-Amy, both free and in complex with AAs. The results are reported in Table 7.

Free α-Glu contained 16.3% β-sheet (1616 cm^{-1}), 27.5% α-helix (1647 cm^{-1}), 27.9% random coil (1631 cm^{-1}), 19.0% β-turn (1663 cm^{-1}), and 9.3% β-antiparallel (1679 cm^{-1}) structures. After the addition of AAs, β-sheet and random coil contents decreased, whereas α-helix, β-turn, and β-antiparallel contents increased (Table 7).

Free α-Amy consisted of 16.3% β-sheet, 24.7% random coil, 28.8% α-helix, 20.1% β-turn, and 10.1% β-antiparallel structures. After the

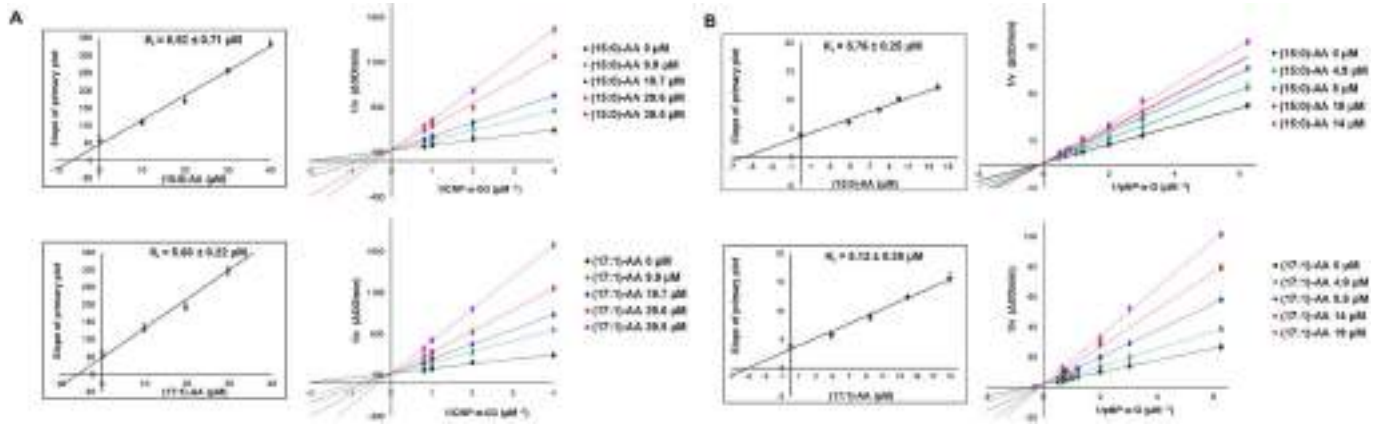

Fig. 3. A–B. Lineweaver-Burk plots of A) α-Amy inhibition at different concentrations of substrate (CNP-α-G3) and B) α-Glu inhibition at different concentrations of substrate (pNP-α-G) in the presence of (15:0)-AA and (17:1)-AA. The insets depict the secondary plot of slope *vs* inhibitor concentration. Plotted data are means ± SD ($n = 3$). K_i, inhibition constant; CNP-α-G3, 2-chloro-4-nitrophenyl-α-maltotrioside; pNP-α-G, *p*-nitrophenyl-α-D-glucopyranoside.

Table 5
Kinetic data on α-amylase (α-Amy) and α-glucosidase (α-Glu) inhibition by (15:0)-AA and (17:1)-AA.

Compound	α-Amy		α-Glu	
	Inhibition type	$K_i = \pm$ SD (μM)	Inhibition type	$K_i = \pm$ SD (μM)
(15:0)-AA	Competitive	6.52 ± 0.71^{b}	Competitive	5.76 ± 0.25^{b}
(17:1)-AA	Competitive	5.68 ± 0.22^{c}	Competitive	5.12 ± 0.38^{c}
Acarbose*	Competitive	23.56 ± 0.84^{a}	Competitive	179.32 ± 11.5^{a}

K_i = competitive inhibition constant estimated by secondary plots of slope *vs* inhibitor concentrations.
Different letters in the same column indicate significant differences (Tukey's test, $p < 0.05$). Results are reported as mean ± SD ($n = 3$).
* Reference standard [1].

addition of AAs, α-helix and β-sheets contents decreased, while the random coil, β-antiparallel, and β-turn contents increased (Table 7).

3.6.2. *Dynamic light scattering (DLS) experiments*

The binding properties of enzyme-inhibitor systems were studied by DLS (Fig. S5), a technique that provides qualitative information on the size distribution of proteins and their aggregates resulting from protein–small molecule interactions. In the studied medium, α-Glu exhibited an average hydrodynamic diameter of 23.94 nm and a polydispersity index (PDI) of 0.17, indicating a homogeneous solution.

The interaction between α-Glu and both the AAs resulted in an increased size distribution, reaching 63.22 nm in the presence of (17:1)-AA and 60.57 nm in the presence of (15:0)-AA after 15 min of incubation at 37 °C. Analogously, α-Amy exhibited a size of 113.6 nm and a PDI of

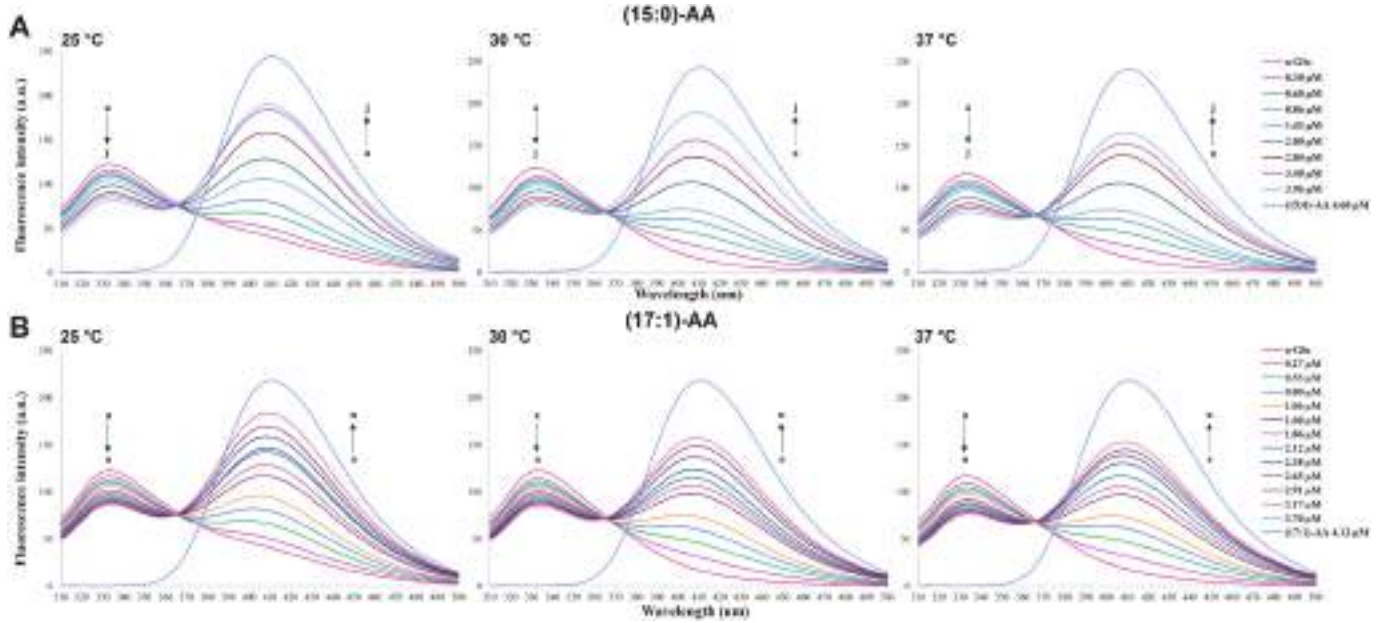

Fig. 4. A–B. Changes in the intrinsic α-Glu fluorescence at different concentrations (0–3.70 μM) of A) (15:0)-AA and B) (17:1)-AA observed at three different temperatures (pH 6.9, $\lambda_{ex} = 295$ nm).

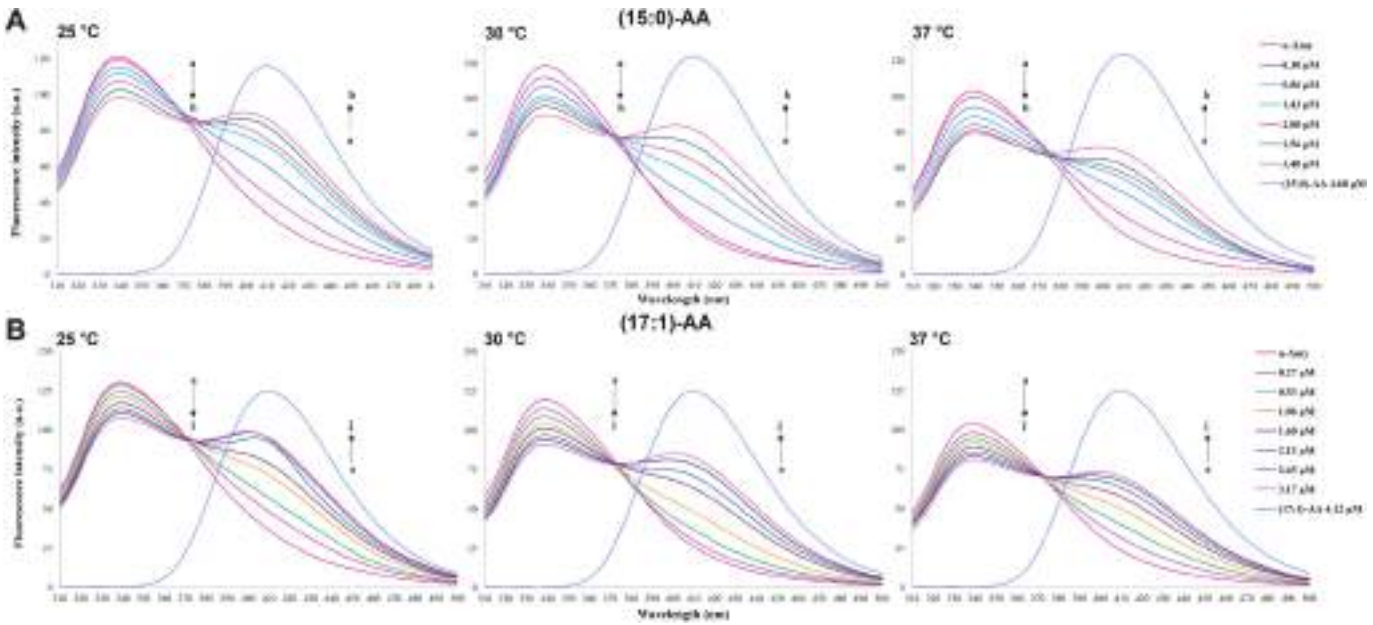

Fig. 5. A–B. Changes in the intrinsic α-Amy fluorescence at different concentrations (0–3.70 μM) of A) (15:0)-AA and B) (17:1)-AA observed at three different temperatures (pH 6.9, $\lambda_{ex} = 295$ nm).

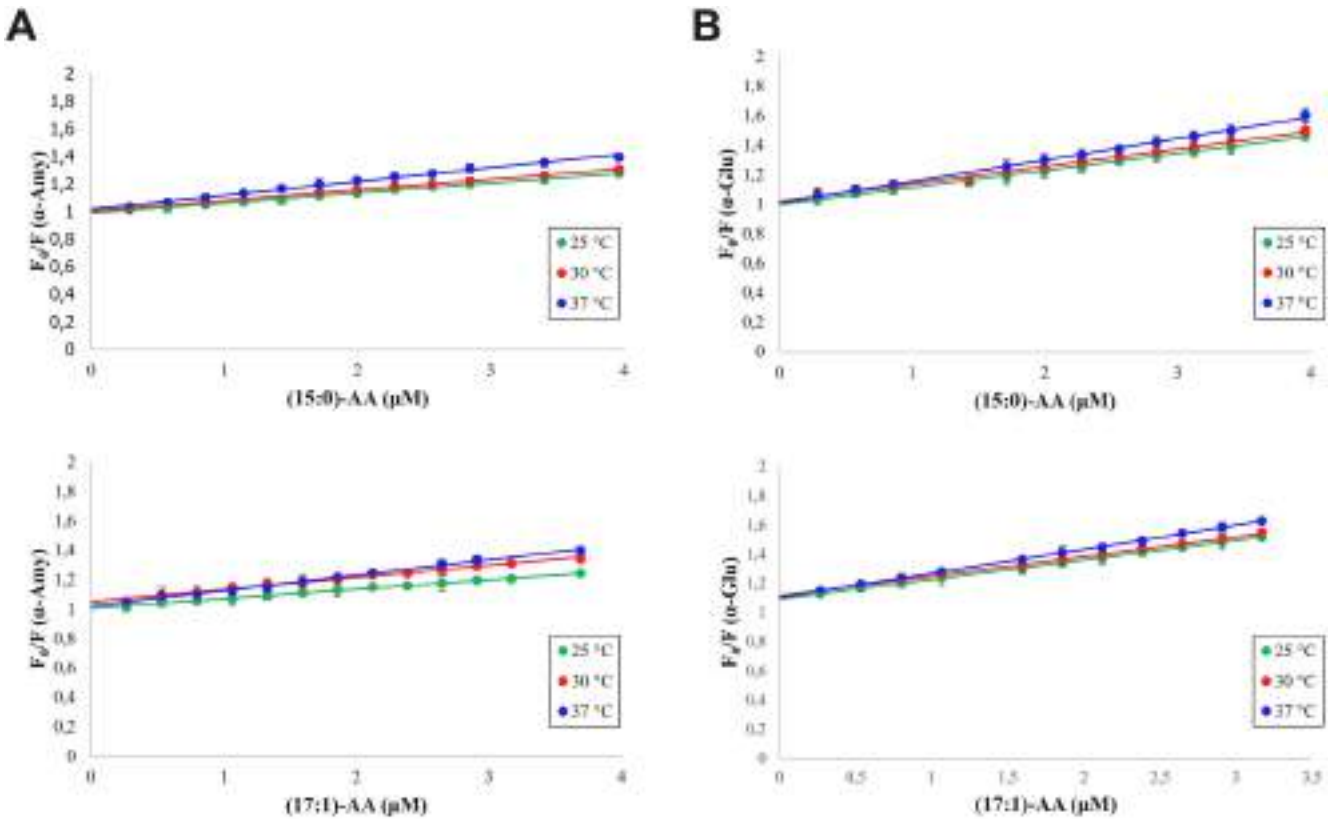

Fig. 6. A–B. Stern-Volmer plots for the quenching effects of α-Amy (A) and α-Glu (B) with (15:0)-AA and (17:1)-AA.

0.32. Interaction with (17:1)-AA and (15:0)-AA caused an increase of this parameter, reaching values of 163.6 nm and 150.8 nm, respectively. The increases in particle size suggest the occurrence of binding interactions between AAs and the two enzymes, leading to conformational changes responsible for the observed size variations [50].

3.7. Effects of anacardic acids (AAs) on advanced glycation end products (AGEs) formation

Prolonged exposure to elevated levels of reducing sugars promotes glycation, a non-enzymatic chemical modification of biological macromolecules, including proteins, DNA, and lipids [50,51]. This multistage process begins with the formation of Schiff bases and Amadori products

Table 6
Stern–Volmer quenching constant (K_{SV}), binding constant (K_a) and number of binding sites (n) for the interaction of (15:0)-AA and (17:1)-AA with α-amylase (α-Amy) and α-glucosidase (α-Glu). Results are reported as mean ± SD (n = 3).

	T (°C)	K_{SV} (×10^4 L/mol)	R^2	K_a (× 10^5 L/mol)	n	R^2
α-Glu						
	25	11.54 ± 0.01	0.9940	1.04 ± 0.01	1.10	0.9996
(15:0)-AA	30	11.78 ± 0.06	0.9942	1.19 ± 0.03	1.05	0.9977
	37	14.50 ± 0.05	0.9980	1.44 ± 0.03	1.02	0.9971
	25	12.51 ± 0.02	0.9976	1.05 ± 0.01	1.11	0.9965
(17:1)-AA	30	12.88 ± 0.04	0.9930	1.09 ± 0.04	1.18	0.9957
	37	16.55 ± 0.02	0.9981	1.47 ± 0.08	1.01	0.9994
α-Amy						
	25	7.28 ± 0.03	0.9957	0.60 ± 0.03	1.13	0.9977
(15:0)-AA	30	7.66 ± 0.02	0.9982	0.74 ± 0.01	1.05	0.9958
	37	10.03 ± 0.04	0.9928	1.22 ± 0.04	1.00	0.9986
	25	6.44 ± 0.02	0.9948	0.57 ± 0.03	1.18	0.9939
(17:1)-AA	30	8.25 ± 0.01	0.9901	0.92 ± 0.04	1.02	0.9995
	37	10.40 ± 0.04	0.9930	1.01 ± 0.06	1.25	0.9913

(early-stage glycation), followed by oxidative reactions that produce reactive carbonyl species like MGO, ultimately leading to AGEs formation (middle to advanced-stage glycation). AGEs, in turn, contribute to oxidative stress and are closely related to T2DM progression, vascular complications and atherosclerosis, among other disorders [22,52].

In this study, the effects of (15:0)-AA and (17:1)-AA on AGEs production were screened for the first time using three complementary *in vitro* models, namely HSA/fructose, HSA/methylglyoxal (MGO), and Arg/MGO, to mimic different stages of protein glycation [33]. AAs were tested at five different concentrations to determine the IC_{50} values. Hence, the formation of total fluorescent AGEs was monitored by fluorescence spectroscopy at λ_{ex} = 340 nm; λ_{em} = 420 nm, while the formation of the AGE Arg-pyrimidine was monitored at λ_{ex} = 340 nm; λ_{em} = 380 nm [33]. The results, expressed as inhibitory percentages and IC_{50} values (μg/mL), are reported in Fig. 8A–C.

All results were compared with those of catechin, a well-recognized natural inhibitor of protein glycation [33,53]. Additionally, AG, a synthetic inhibitor discontinued from clinical trials due to serious adverse effects, was also tested as a positive control. As expected, this latest showed the highest antiglycation activity (Fig. 8A–C), attesting to the robustness of all the employed reaction models [33]. According to Fig. 8A–C, both AAs showed appreciable inhibitory capacity against total fluorescent AGEs formation.

Table 7
Secondary structure content determined by FT-IR of α-glucosidase (α-Glu) and α-amylase (α-Amy) in the absence and presence of anacardic acids (AAs).

Enzyme/AA	β-Sheet	Random coil	α-Helix	β-Turn	β-Antiparallel
α-Glu					
1:0	16.3%	27.9%	27.5%	19.0%	9.3%
1:10 (15:0)-AA	12.3%	24.2%	28.1%	23.9%	12.5%
1:10 (17:1)-AA	13.4%	25.7%	28.1%	21.5%	11.3%
α-Amy					
1:0	16.3%	24.7%	28.8%	20.1%	10.1%
1:10 (15:0)-AA	12.5%	25.2%	28.1%	22.4%	11.8%
1:10 (17:1)-AA	14.4%	26.7%	28.1%	20.4%	10.4%

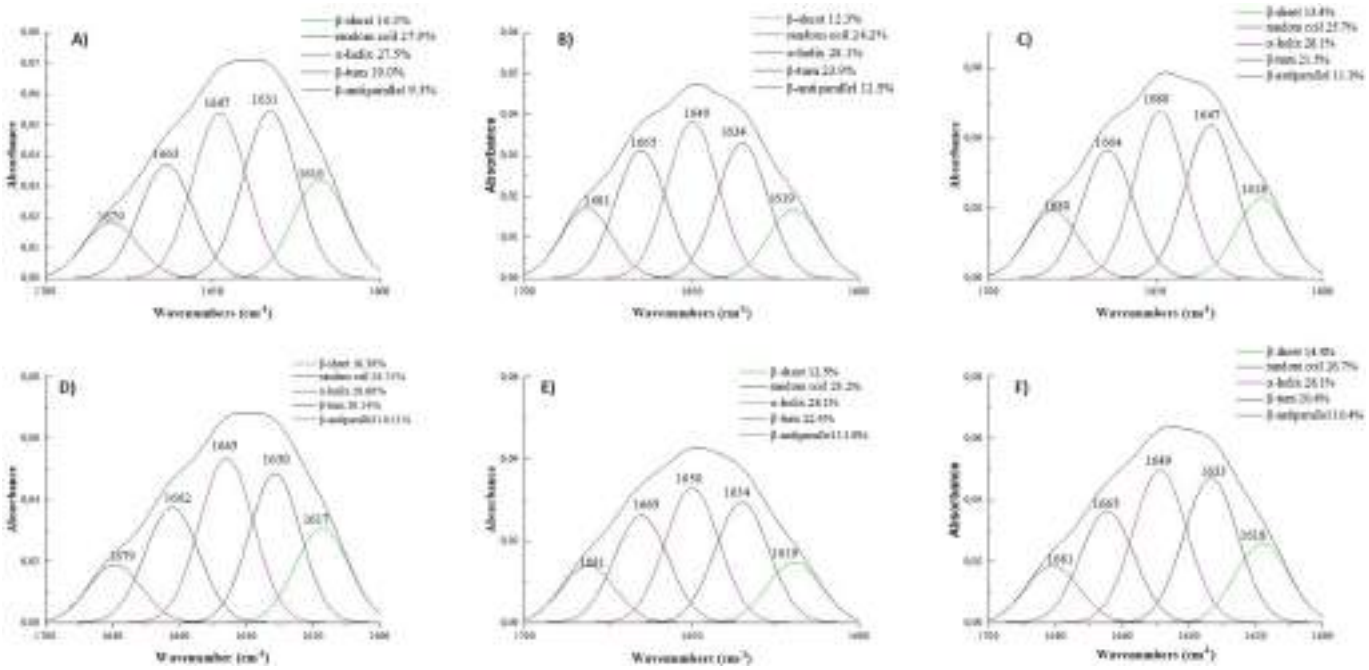

Fig. 7. A–F. The curve-fitted of FT-IR spectra (amide I region, 1700–1600 cm^{-1}) of: A) free α-Glu, B) α-Glu-(15:0)-AA complex, C) α-Glu-(17:1)-AA complex, D) free α-Amy, E) α-Amy-(15:0)-AA complex, F) α-Amy-(17:1)-AA complex.

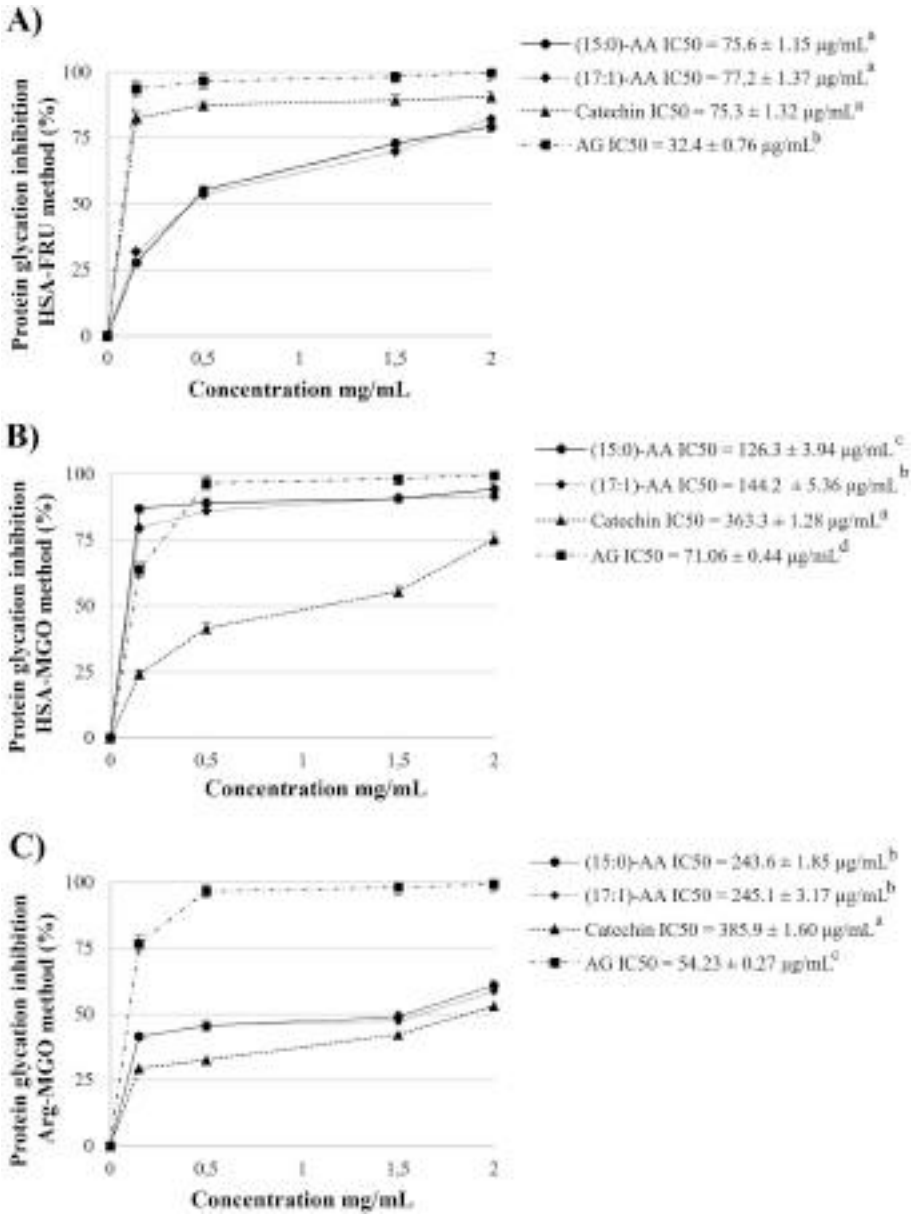

Fig. 8. A–B. Inhibitory effects of (15:0)-AA and (17:1)-AA on total fluorescent AGEs formation using (A) human serum albumin-fructose (HSA-FRU), (B) HSA-methylglyoxal (HSA-MGO) and (C) arginine-methylglyoxal (Arg-MGO) reaction models, respectively. Results are means ± SD. IC_{50} is the concentration required to inhibit 50% of protein glycation. Different letters indicate significant differences ($p < 0.05$, Tukey's test).

The HSA/FRU model evaluated the ability of AAs to inhibit the early, sugar-driven stage of protein glycation. As shown in Fig. 8A, the inhibitory capacity of (15:0)-AA and (17:1)-AA was not significantly different ($p > 0.05$) from that of the pure compound catechin (IC_{50} = 75.3 μg/mL), as highlighted by their IC_{50} values of 75.6 μg/mL and 77.2 μg/mL, respectively. Furthermore, compared with AG, AAs inhibited AGEs formation in a concentration-dependent manner, showing inhibition percentages ranging from 27.68% to 79.28% for (15:0)-AA, and from 31.87% to 82.27% for (17:1)-AA, respectively, at 0.15 mg/mL and 2 mg/mL.

The HSA/MGO model tested the ability of AAs to trap MGO, one of the most reactive dicarbonyl compounds, and inhibit the intermediate to late stages of glycation. In this model, both AAs acted as effective MGO scavengers with inhibition percentages higher than 79.57% even at the lowest tested concentration (Fig. 8B). Moreover, the inhibitory efficacy of (15:0)-AA (IC_{50} = 126.3 μg/mL) and (17:1)-AA (IC_{50} = 144.2 μg/mL) towards AGEs formation was significantly ($p > 0.05$) higher than that of catechin (IC_{50} = 363.3 μg/mL) and almost comparable with that of AG (IC_{50} = 71.06 μg/mL). The results observed in the HSA/MGO reaction model suggest that AAs could prevent fluorescent AGEs formation by trapping MGO and other key reactive carbonyl species in the glycosylation process.

Lastly, the site-specific Arg/MGO model reflected direct carbonyl–amino acid interactions without the complexity of protein structure. As shown in Fig. 8C, (15:0)-AA (IC_{50} = 243.6 μg/mL) and (17:1)-AA (IC_{50} = 245.1 μg/mL) acted as significantly ($p > 0.05$) more efficient inhibitors of Arg-pyrimidine formation than catechin (IC_{50} = 485.9 μg/mL, 53.12%), exhibiting inhibition percentages of 60.83% and 58.61%, respectively, at the highest tested concentration (2 mg/mL).

3.8. Antiglycation studies on human serum albumin (HSA)

3.8.1. Effects of AAs on the stability of protein structure

MGO is one of the most reactive intermediates of glucose metabolism

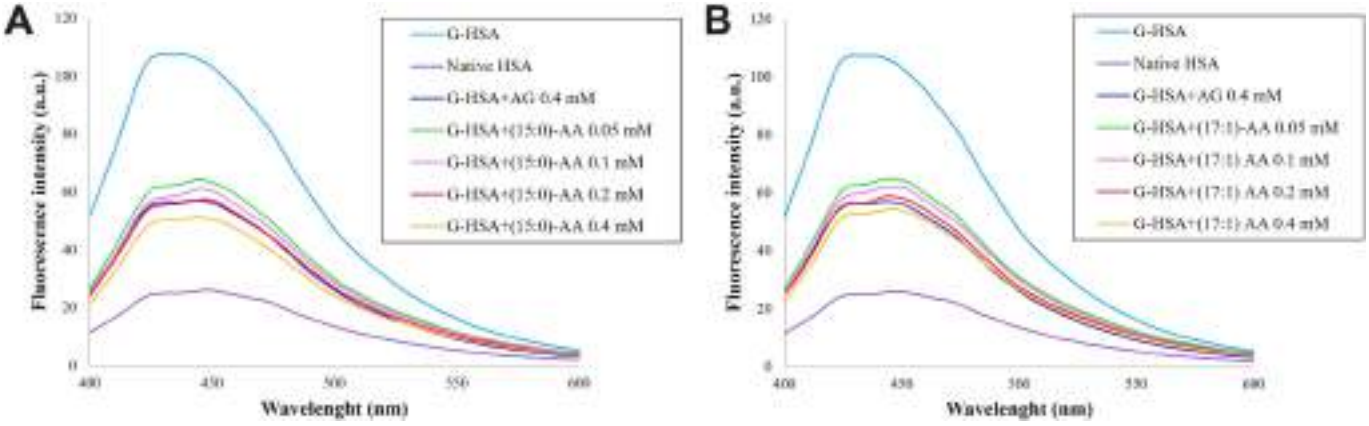

Fig. 9. A–B. Fluorescence spectra of native and glycated human serum albumin (G-HSA), as well as G-HSA treated with (A) (15:0)-AA and (B) (17:1)-AA excited at 370 nm. Aminoguanidine (AG) was tested as a positive control.

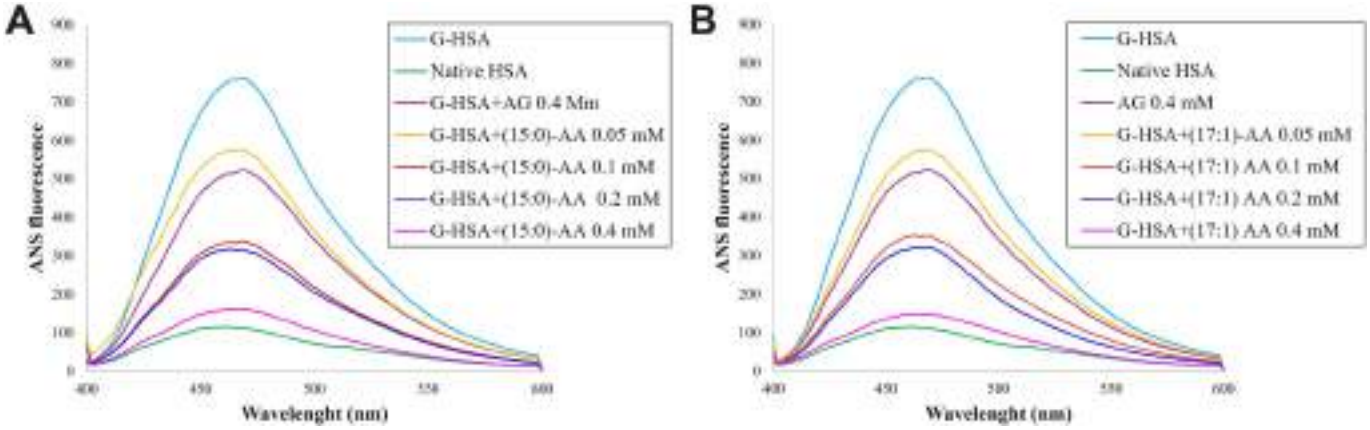

Fig. 10. A–B. Fluorescence spectra of 1-anilinonaphthalene-8-sulfonate (ANS) binding to native and glycated human serum albumin (G-HSA), as well as to G-HSA treated with (A) (15:0)-AA and (B) (17:1)-AA excited at 385 nm. Aminoguanidine (AG) was tested as a positive control.

and is known for inducing structural and conformational changes in HSA [35,37], including partial unfolding and aggregation into toxic amyloid fibrils. In this study, fluorescence measurements were performed to assess the ability of AAs to inhibit MGO-induced alterations in the conformation of the native protein. The intrinsic fluorescence spectra of native HSA, G-HSA, and G-HSA treated with the tested AAs are presented in Fig. 9A–B.

Notably, MGO treatment markedly increased HSA fluorescence intensity, with an emission peak at 440 nm, consistent with the formation of fluorogenic AGEs, which typically exhibit emission maxima around

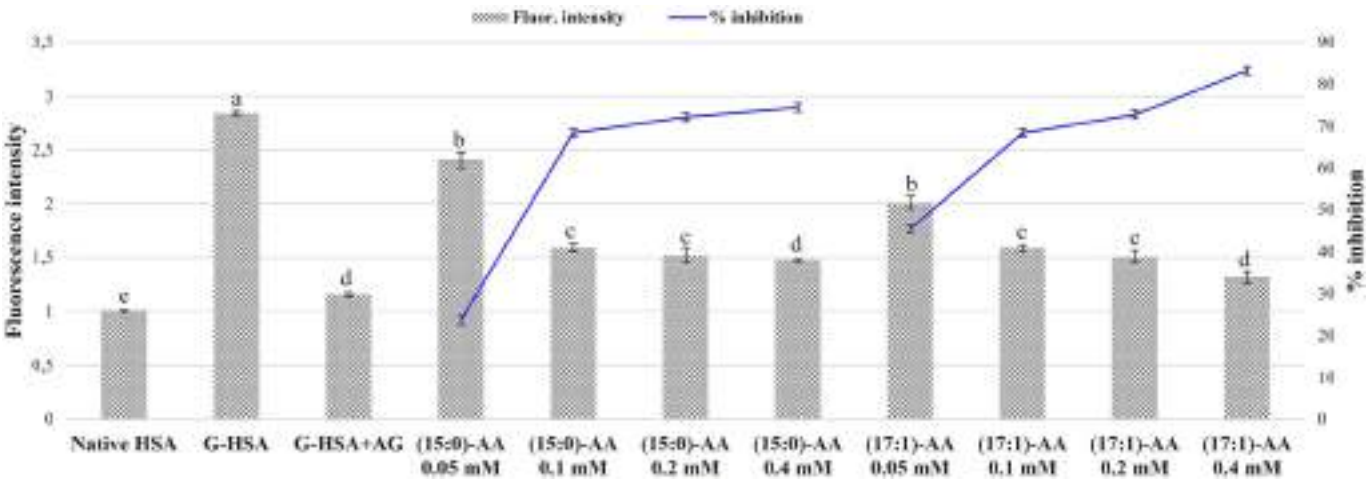

Fig. 11. Inhibition of glycation-induced amyloid formation in human serum albumin (HSA) and ThT fluorescence intensities ($\lambda_{ex} = 430$ nm; $\lambda_{em} = 485$ nm) of native and glycated HSA (G-HSA), as well as G-HSA treated with different concentrations (0.05, 0.1, 0.2, and 0.4 mM) of (15:0)-AA and (17:1)-AA. Different letters above error bars represent significant differences (Tukey's test; $p < 0.05$). Results are reported as mean ± SD ($n = 3$).

445 nm [37]. A similar increase in intrinsic protein fluorescence has also been reported by Qais et al. for MGO-modified HSA [35].

Treatment of G-HSA with increasing concentrations of tested AAs resulted in a dose-dependent reduction in fluorescence intensity, as also observed for AG, used as a positive control (Fig. 9A–B). These results suggest that (15:0)-AA and (17:1)-AA can effectively counteract MGO-induced structural changes in native HSA by interacting with reactive carbonyl intermediates or by protecting vulnerable amino acid residues from modification.

To further investigate the ability of AAs to prevent MGO-induced alterations in HSA's conformation, we measured ANS binding to the modified HSA (Fig. 10A–B). ANS is a fluorophore that exhibits strong fluorescence upon binding to hydrophobic domains [54], making it a widely used probe for monitoring changes in protein binding sites [55]. In albumin, glycation has been reported to induce partial unfolding and conformational loosening, increasing the exposure of hydrophobic domains [22].

According to Fig. 10A–B, glycated samples exhibited a higher ANS fluorescence intensity compared with native HSA, reflecting increased exposure of hydrophobic regions caused by glycation. This observation is consistent with previous studies reporting enhanced ANS fluorescence in G-HSA compared to its native form [35,56]. Treatment with increasing concentrations of tested AAs resulted in reduced ANS binding (Fig. 10 A–B), indicating that the protein adopted a more compact structure. These findings suggest that AAs, similarly to AG [35], mitigate glycation-driven exposure of hydrophobic regions and can help maintain the native-like structure of HSA under glycation conditions.

3.8.2. *Effect of AAs on MGO-induced cross-linking and aggregation of HSA*

Numerous studies have shown that glycation alters albumin's colloidal stability, promoting its aggregation in amyloid fibrils, protein aggregates with a needle-shape geometry [22]. In contrast to its native helical structure, G-HSA exhibits an amyloid cross-β structure with strong affinity for ThT, an amyloid-specific benzothiazole dye [22]. In this study, the inhibitory effect of AAs on the formation of HSA amyloid fibrils was investigated by measuring the ThT fluorescence emission upon binding to native HSA, G-HSA, and G-HSA treated with different concentrations of (15:0)-AA and (17:1)-AA. Results are presented in Fig. 11.

G-HSA exhibited a remarkably higher fluorescence compared to native HSA, indicating the presence of amyloid fibrils and cross-β structures. G-HSA treatment with 0.05, 0.1, 0.2, and 0.4 mM (15:0)-AA significantly reduced ThT fluorescence and inhibited amyloid formation by 25.2%, 72.7%, 76.3%, and 85.4%, respectively. Similarly, treatment with 0.05, 0.1, 0.2, and 0.4 mM (17:1)-AA significantly inhibited HSA fibrillation by 48.3%, 73.8%, 77.3%, and 88.5%, respectively (Fig. 11). The reduction in ThT fluorescence intensity of G-HSA suggested that both AAs can effectively protect HSA from fibrillation and aggregation, thereby uncovering for the first time their anti-amyloidogenic role under glycation conditions.

3.8.3. *Ability of AAs to capture dicarbonyl compounds*

Reactive dicarbonyl compounds, such as MGO, are generated in large amounts during non-enzymatic glycation and are precursors of highly toxic AGEs [22]. In this study, the amount of dicarbonyl compounds was estimated in both native HSA and glycated samples. The results are shown in Fig. 12.

As expected, G-HSA showed a much higher amount of dicarbonyl compounds (37.42 ± 2.5 mol/mol HSA) compared to native HSA, which showed a negligible dicarbonyl content (3.98 n mol/mg of protein). Noteworthy, dicarbonyl content in G-HSA was significantly ($p < 0.05$) reduced in the presence of (15:0)-AA (25.8 ± 1.1 mol/mol HSA) and (17:1)-AA (19.1 ± 1.2 mol/mol HSA). These results demonstrate the AAs' ability to quench dicarbonyl compounds.

3.8.4. *Evaluation of HSA structural alterations by FT-IR spectroscopy*

The changes in the native conformation of HSA induced by MGO were further explored by FT-IR measurements. Fig. 13A–D reports the curve fitting of FT-IR spectra of native HSA, G-HSA and G-HSA complexes with (15:0)-AA and (17:1)-AA in the range of 4500–400 cm^{-1} [57]. The relative content of each secondary structure element in native HSA and its glycated forms was calculated from curve fitting of the amide I region, and the results are reported in Table 8. Both (15:0)-AA and (17:1)-AA were tested at a concentration of 0.4 mM, which showed the highest antiglycation activity (Fig. 9A-B).

In the main bands of the HSA IR spectra, the amide I peak, which is primarily associated with the C═O stretching vibrations of the peptide backbone, appears in the 1700–1600 cm^{-1} region [57,58]. In native HSA, the secondary structure was composed of 9.99% β-sheet (1615 cm^{-1}), 27.84% random coil (1630 cm^{-1}), 29.60% α-helix (1645 cm^{-1}), 21.73% β-turn (1662 cm^{-1}), and 10.86% β-antiparallel (1679 cm^{-1}). Upon MGO-induced glycation, an increase in β-sheet (+1.48%), β-turn (+1.18), and β-antiparallel (+1.61) structures was observed, indicating partial unfolding and aggregation of the protein. Conversely, the proportions of random coil and α-helix structures in G-HSA were significantly reduced (−3.4% and −0.89%, respectively). Both AAs effectively reduced these structural alterations. Treatment with (15:0)-AA (−2.63% and −0.37%, respectively) and (17:1)-AA (−2.88% and −0.17%, respectively) limited these decreases, preserving a more balanced secondary-structure profile. These findings suggest that both (15:0)-AA and (17:1)-AA can help preserve a more native-like conformation of HSA under glycation conditions, consistent with the fluorescence results.

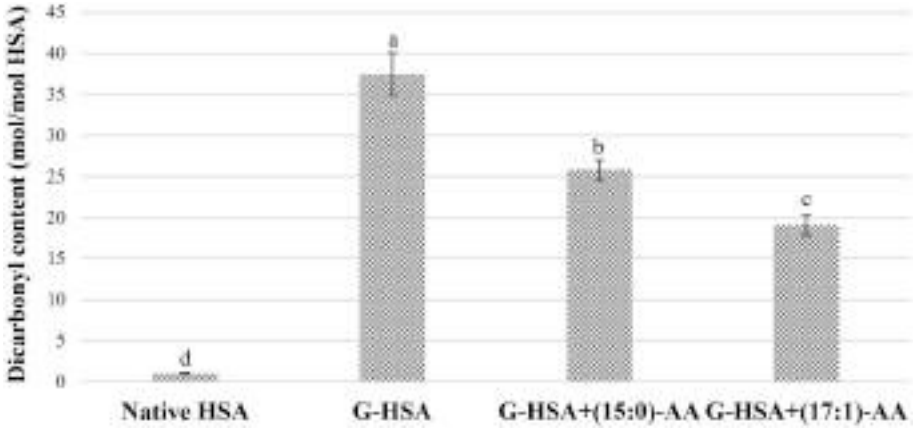

Fig. 12. Ability of (15:0)-AA and (17:1)-AA to trap dicarbonyl compounds. Results are reported as mean ± SD ($n = 3$). Different letters above error bars represent significant difference (Tukey's test; $p < 0.05$).

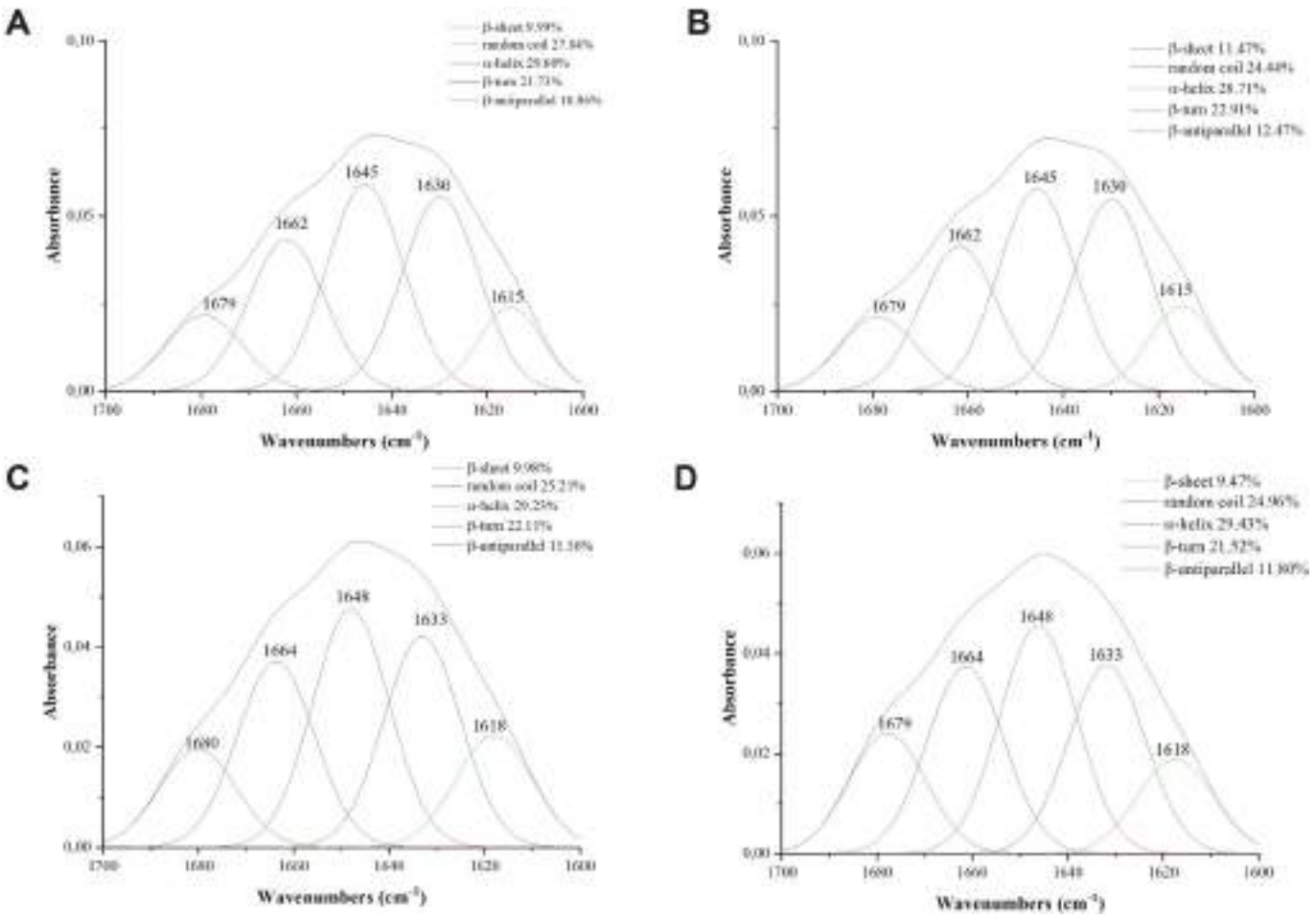

Fig. 13. A–D. The curve-fitting of FT-IR spectra (amide I region, 1700–1600 cm^{-1}) of: (A) native HSA, (B) glycated HSA (G-HSA), (C) G-HSA/(15:0)-AA complex and (D) G-HSA/(17:1)-AA complex.

Table 8
Secondary structure composition of native HSA, glycated HSA (G-HSA) and G-HSA treated with 0.4 mM (15:0)-AA and (17:1)-AA.

Conformation	HSA	G-HSA	G-HSA + (15:0) AA	G-HSA + (17:1) AA
β-Sheet	9.99%	11.47% (+1.48%)	9.98% (−0.01%)	9.47% (−0.52)
Random coil	27.84%	24.44% (−3.4%)	25.21% (−2.63)	24.96% (−2.88)
α-Helix	29.60%	28.71% (−0.89%)	29.23% (−0.37)	29.43% (−0.17)
β-Turn	21.73%	22.91% (+1.18%)	22.11% (+0.38)	21.52% (−0.21)
β-Antiparallel	10.86%	12.47% (+1.61%)	11.56% (+0.7)	11.80% (+0.94)

3.8.5. Antiglycation activity of AAs after in vitro digestion

In our previous study, *in vitro* simulated digestion and untargeted metabolomic analysis were performed on the AA-rich PVS-E [41]. Despite a decrease in concentration, AAs remained stable in the gastrointestinal environment, suggesting that they may retain their bioactivity even after digestion [41]. In the present study, AAs were subjected for the first time to the standardized INFOGEST digestion protocol developed by Minekus et al. [40], and their antiglycation effect after digestion was evaluated using the HSA/MGO glycation model, in which undigested AAs had shown inhibition percentages higher than 79.57% even at the lowest tested concentration (Fig. 8B). The inhibitory activity of undigested and digested AAs on AGE formation is shown in Fig. 18A.

According to Fig. 14A, the inhibitory efficacy of AAs significantly ($p > 0.05$) decreased by 1.8-fold and 1.5-fold after oral and gastric digestion, respectively, and by 2.5-fold after intestinal digestion. Specifically, the AGE inhibition rates of (15:0)-AA and (17:1)-AA increased slightly from 53.8% and 58.4% in the oral phase to 54.4% and 60.5% in the gastric phase and subsequently decreased to 33.3% and 22.5% in the intestinal phase, respectively. This decrease in the intestinal phase could be related to the lower stability of AAs under alkaline conditions, which was previously reported [40]. A similar trend has also been observed for the antiglycation activity of catechins and ferulic acid, which exhibited higher AGE inhibitory effects during the gastric phase compared with the intestinal stage [42].

Fig. 14B shows the fluorescence intensity of digested G-HSA and G-HSA treated with AAs. The fluorescence intensity of G-HSA significantly ($p < 0.05$) increased throughout digestion, reaching its maximum during the intestinal phase. This can be attributed to the deprotonation of lysine amino groups at higher pH values, which increases HSA nucleophilicity and enhances its interaction with reactive carbonyls such as MGO, thereby promoting AGE release [59]. However, the treatment with AAs markedly reduced G-HSA fluorescence intensity at all digestion stages, indicating that they could effectively inhibit AGE formation during simulated gastrointestinal digestion.

Although the INFOGEST gastrointestinal digestion protocol is a

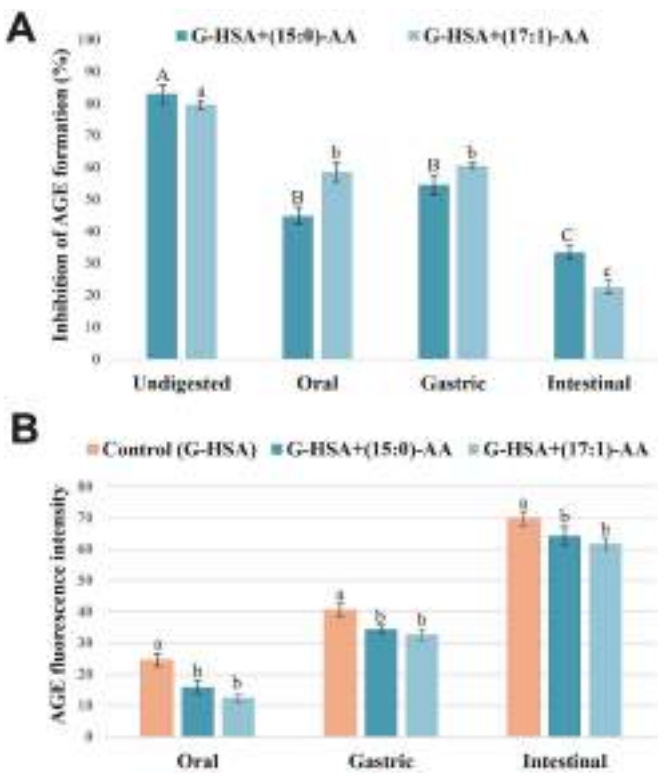

Fig. 14. A–B. (A) The inhibitory activity of AAs on MGO-mediated AGE formation before and after *in vitro* simulated digestion. (B) AGE fluorescence intensities of glycated HSA (G-HSA) and G-HSA treated with (15:0)-AA and (17:1)-AA in the oral, gastric, and intestinal digestive stages. Results are reported as mean ± SD ($n = 4$). Different letters in the same group represent significant differences (Tukey's test; $p < 0.05$).

widely accepted, standardized model, it does not fully mimic the dynamic processes of human digestion, absorption, metabolism, and microbiota interactions. Future cell-based permeability assays and *in vivo* pharmacokinetic studies should be performed to evaluate inter-individual variability or gut microbiota-mediated metabolic transformations, thereby determining the actual intestinal absorption, systemic bioavailability and effects of AAs.

4. Conclusion

In summary, this study provided the first comprehensive investigation of the inhibitory mechanisms and antiglycation properties of AAs against key enzymes implicated in T2DM. Fraction F4, including 85.69% of the total AAs quantified in PVS-E and characterized by a high content of (15:0)-AA and (17:1)-AA, exhibited the most potent α-Amy and α-Glu inhibitory activity, overcoming the reference drug acarbose. Kinetic and molecular docking analyses demonstrated that both AAs can act as competitive inhibitors of both the enzymes, effectively binding to their catalytic sites through non-covalent interactions involving both the salicylic portion and aliphatic side chain. FT-IR measurements revealed the changes of the secondary structure of α-Glu and α-Amy upon interaction with tested AAs, highlighting rearrangement of the hydrogen bonding pattern. DLS experiments corroborated the occurrence of binding interactions between AAs and the two enzymes, resulting in increased size distribution. Fluorescence measurements allowed for the first time to estimate the quenching and binding constants for (15:0)-AA and (17:1)-AA with α-Amy and α-Glu, highlighting the occurrence of dynamic quenching.

Beyond their hypoglycaemic activity, AAs displayed remarkable *in vitro* antiglycation effects, showing inhibitory efficacy comparable to or greater than catechin and AG. Both (15:0)-AA and (17:1)-AA efficiently prevented the formation of fluorescent AGEs, mitigated the exposure of HSA hydrophobic regions, and protected HSA from glycation-induced fibrillation and aggregation, thereby preserving its structural integrity under glycation conditions.

Using multi-spectroscopic and *in silico* techniques, this study provided a robust mechanistic foundation for the application of AAs as novel multifunctional ingredients, setting the stage for future translational research. Although promising, the *in vitro* and *in silico* findings cannot fully reproduce the complexity of physiological conditions occurring *in vivo*. For instance, the effective *in vitro* concentrations identified herein may not directly reflect achievable plasma or tissue levels following an oral intake. Future studies should therefore include *in vivo* investigations, pharmacokinetic analyses, and safety assessments to better define the therapeutic potential of AAs. Furthermore, innovative formulation strategies, including nano-delivery systems, may be explored to improve the solubility and gastrointestinal bioavailability of such lipophilic compounds. In this context, potential synergistic effects among different AAs or in conjunction with conventional hypoglycemic drugs such as acarbose should also be considered. All these steps will be fundamental to fully exploit AAs as novel multifunctional ingredients for the management of T2DM and its related complications.

CRediT authorship contribution statement

Anna Elisabetta Maccarronello: Writing – original draft, Validation, Methodology, Investigation, Formal analysis. **Claudia Sciacca:** Visualization, Methodology. **Nunzio Cardullo:** Writing – review & editing, Visualization, Validation, Supervision, Methodology. **Luana Pulvirenti:** Validation, Investigation, Formal analysis. **Antonella Di Francesco:** Visualization, Methodology, Formal analysis. **Vera Muccilli:** Writing – review & editing, Visualization, Supervision, Resources, Project administration, Funding acquisition, Conceptualization.

Funding

This research was financed by: PRIN 2022 PNRR (P2022MWY3P) macrosettore "PE - Physical Sciences and Engineering" Title: "Old but Gold! Identification of molecular platforms for age-associated diseases to promote healthy and active aging." D.D. 1409 del 14/09/2022 - PNRR per la Missione 4, Componente 2, Investimento 1.1; the University of Catania, PIAno di inCEntivi per la RIcerca di Ateneo (PIACERI) 2020/2022, Linea di Intervento 3 "Starting Grant" project HYPOGLYCEMIA; the University of Catania PIACERI 2024/2026, Linea di Intervento 1, project "NanoBioIn - Sviluppo di nanobiopesticidi basati su argille minerali per applicazioni in agricoltura".

Declaration of competing interest

The authors declare that they have no known competing financial interests or personal relationships that could have appeared to influence the work reported in this paper.

Acknowledgements

The authors gratefully acknowledge the Bio-Nanotech Research and Innovation Tower of the University of Catania (BRIT; project PONa3_00136) financed by the Italian Ministry for Education, University and Research MIUR, for making available the Synergy H1 microplate reader and Varioskan Flash multimode reader.

Appendix A. Supplementary data

Supplementary data to this article can be found online at https://doi.org/10.1016/j.ijbiomac.2026.152760.

Data availability

Data will be made available on request.

References

[1] C. Sciacca, N. Cardullo, L. Pulvirenti, G. Travagliante, A. D'Urso, R. D'Agata, E. Peri, P. Cancemi, A. Cornu, D. Deffieux, L. Pouységu, S. Quideau, V. Muccilli, Synthesis of obovatol and related neolignan analogues as α-glucosidase and α-amylase inhibitors, Bioorg. Chem. 147 (2024) 107392, https://doi.org/10.1016/j.bioorg.2024.107392.

[2] S.M. Morais, K.A. Silva, H. Araujo, I.G.P. Vieira, D.R. Alves, R.O.S. Fontenelle, A.M. S. Silva, Anacardic acid constituents from cashew nut shell liquid: NMR characterization and the effect of unsaturation on its biological activities, Pharmaceuticals (Basel) 10 (1) (2017) 31, https://doi.org/10.3390/ph10010031.

[3] M.M. Ng'ang'a, H. Hussain, S.C. Chhabra, C. Langat-Thoruwa, K. Krohn, Chemical constituents from the root bark of *Ozoroa insignis*, Biochem. Syst. Ecol. 37 (2) (2009) 116–119, https://doi.org/10.1016/j.bse.2008.11.019.

[4] M. Akyuz, L. Yabo-Dambagi, B. Simitcioglu, I.D. Karagoz, T. Aydin, G. Gokdemir, A. Cakir, C. Kazaz, The chemical composition and antidiabetic, neuroprotective and cytotoxic activities of soft hulls (mesocarp) of pistachio (*Pistacia vera*) fruits, J. Chem. Soc. Pak. 45 (6) (2023) 551–567, https://doi.org/10.52568/001397/JCSP/45.06.2023.

[5] A.E. Maccarronello, N. Cardullo, A.M. Silva, A. Di Francesco, P.C. Costa, F. Rodrigues, V. Muccilli, From waste to bioactive compounds: a response surface methodology approach to extract antioxidants from *Pistacia vera* shells for postprandial hyperglycaemia management, Food Chem. 443 (2024) 138504, https://doi.org/10.1016/j.foodchem.2024.138504.

[6] S. Ersan, Ö.G. Üstündağ, R. Carle, R.M. Schweiggert, Subcritical water extraction of phenolic and antioxidant constituents from pistachio (*Pistacia vera* L.) hulls, Food Chem. 253 (2018) 46–54, https://doi.org/10.1016/j.foodchem.2018.01.116.

[7] S. Ersan, Ö.G. Üstündağ, R. Carle, R.M. Schweiggert, Determination of pistachio (*Pistacia vera* L.) hull (exo- and mesocarp) phenolics by HPLC-DAD-ESI/MS^n and UHPLC-DAD-ELSD after ultrasound-assisted extraction, J. Food Compos. Anal. 62 (2017) 103–114, https://doi.org/10.1016/j.jfca.2017.04.013.

[8] V. Muccilli, A.E. Maccarronello, C. Rasoanandrasana, N. Cardullo, M.S. de Luna, M. G.G. Pittalà, P.M. Riccobene, S.C. Carroccio, A.A. Scamporrino, Green^3: a green extraction of green additives for green plastics, Heliyon 10 (2) (2024) e24469, https://doi.org/10.1016/j.heliyon.2024.e24469.

[9] Y. Hu, W. Xu, L. Wang, Y. He, Y. Zhao, Anacardic acid derivatives with significant α-glucosidase inhibitory activity from Syzygium samarangense, Phytochem. Lett. 61 (2024) 75–77, https://doi.org/10.1016/j.phytol.2024.03.016.

[10] L.L. Wang, Y. Jia, Z. Pan, W. Mo, B. Hu, Direct analysis of alkylphenols in *Ginkgo biloba* leaves by thermochemolysis-gas chromatography/mass spectrometry in the presence of tetramethylammonium hydroxide, J. Anal. Appl. Pyrolysis 85 (1–2) (2009) 66–71, https://doi.org/10.1016/j.jaap.2008.09.014.

[11] M.T.S. Trevisan, B. Pfundstein, R. Haubner, G. Würtele, B. Spiegelhalder, H. Bartsch, R.W. Owen, Characterization of alkyl phenols in cashew (*Anacardium occidentale*) products and assay of their antioxidant capacity, Food Chem. Toxicol. 44 (2) (2006) 188–197, https://doi.org/10.1016/j.fct.2005.06.012.

[12] F.D. Gondimet, R.M. Ferreira, T.R. Nogueira, D.S. Serra, M.A. de Sousa Rios, A.T. A. Pimenta, F.S.A. Cavalcante, Effects of anacardic acid monoene on the respiratory system of mice submitted to acute respiratory distress syndrome, Rev. Bras 31 (2) (2021) 232–238, https://doi.org/10.1007/s43450-021-00151-8.

[13] F.B. Hamad, E.B. Mubofu, Potential biological applications of bio-based anacardic acids and their derivatives, Int. J. Mol. Sci. 16 (4) (2015) 8569–8590, https://doi.org/10.3390/ijms16048569.

[14] A.L. Gomes Júnior, M.T. Islam, L.A.D. Nicolau, L.K.M. de Souza, T. de Souza Lopes Araújo, G.A.L. de Oliveira, K. de Melo Nogueira, L. da Silva Lopes, J.R. Medeiros, M.S. Mubarak, A.A. de Carvalho Melo-Cavalcante, Anti-inflammatory, antinociceptive, and antioxidant properties of anacardic acid in experimental models, ACS Omega 5 (31) (2020) 19506–19515, https://doi.org/10.1021/acsomega.0c01775.

[15] I. Kubo, T.J. Ha, K. Tsujimoto, F.E. Tocoli, I.R. Green, Evaluation of lipoxygenase inhibitory activity of anacardic acids, Z. Naturforsch. C. J. Biosci. 63 (7–8) (2008) 539–546, https://doi.org/10.1515/znc-2008-7-812.

[16] N. Masuoka, I. Kubo, Characterization of xanthine oxidase inhibition by anacardic acids, Biochim. Biophys. Acta 1688 (3) (2004) 245–249, https://doi.org/10.1016/j.bbadis.2003.12.010.

[17] I. Kubo, I. Kinst-Hori, Y. Yokokawa, Tyrosinase inhibitors from *Anacardium occidentale* fruits, J. Nat. Prod. 57 (4) (1994) 545–551, https://doi.org/10.1021/np50106a021.

[18] R. Tundis, M.R. Loizzo, F. Menichini, Natural products as alpha-amylase and alpha-glucosidase inhibitors and their hypoglycaemic potential in the treatment of diabetes: an update, Mini Rev. Med. Chem. 10 (4) (2010) 315–331, https://doi.org/10.2174/138955710791331007.

[19] F.Q. Liang, K. Meng, X. Pu, Y. Cao, Y. Shi, J. Shi, Deciphering the binding behavior and interaction mechanism of apigenin and α-glucosidase based on multi-spectroscopic and molecular simulation studies, Int. J. Biol. Macromol. 264 (1) (2024) 130535, https://doi.org/10.1016/j.ijbiomac.2024.130535.

[20] M. Toyomizu, S. Sugiyama, R.L. Jin, T. Nakatsu, α-Glucosidase and aldose reductase inhibitors - constituents of cashew, Anacardium occidentale, nut shell liquids, Phytother. Res. 7 (3) (1993) 252–254, https://doi.org/10.1002/PTR.2650070309.

[21] F. Dil, Z. Ranjkesh, M. Goodarzi, A systematic review of antiglycation medicinal plants, Diabetol. Metab. Syndr. 13 (2) (2019) 1225–1229, https://doi.org/10.1016/j.dsx.2019.01.053.

[22] S. Awasthi, N. Saraswathi, Non-enzymatic glycation mediated structure-function changes in proteins: case of serum albumin, RSC Adv. 6 (93) (2016) 90739–90753, https://doi.org/10.1039/C6RA08283A.

[23] N. Cardullo, G. Floresta, A. Rescifina, V. Muccilli, C. Tringali, Synthesis and *in vitro* evaluation of chlorogenic acid amides as potential hypoglycemic agents and their synergistic effect with acarbose, Bioorg. Chem. 117 (2021) 105458, https://doi.org/10.1016/j.bioorg.2021.105458.

[24] N. Cardullo, V. Muccilli, L. Pulvirenti, A. Cornu, L. Pouységu, D. Deffieux, S. Quideau, C. Tringali, *C*-glucosidic ellagitannins and galloylated glucoses as potential functional food ingredients with anti-diabetic properties: a study of α-glucosidase and α-amylase inhibition, Food Chem. 313 (2020) 126099, https://doi.org/10.1016/j.foodchem.2019.126099.

[25] J.C. Yang, X. Wang, C. Zhang, L. Ma, T. Wei, Y. Zhao, X. Peng, Comparative study of inhibition mechanisms of structurally different flavonoid compounds on α-glucosidase and synergistic effect with acarbose, Food Chem. 347 (2021) 129056, https://doi.org/10.1016/j.foodchem.2021.129056.

[26] E. Harder, W. Damm, J. Maple, C. Wu, M. Reboul, J.Y. Xiang, L. Wang, D. Lupyan, M.K. Dahlgren, J.L. Knight, J.W. Kaus, D.S. Carutti, G. Krilov, W.L. Jorgensen, R. Abel, R.A. Friesner, OPLS3: a force field providing broad coverage of drug-like small molecules and proteins, J. Chem. Theory Comput. 12 (1) (2016) 281–296, https://doi.org/10.1021/acs.jctc.5b00864.

[27] Y. Yang, K. Yao, M.P. Repasky, K. Leswing, R. Abel, B.K. Shoichet, S.V. Jerome, Efficient exploration of chemical space with docking and deep learning, J. Chem. Theory Comput. 17 (11) (2021) 7106–7119, https://doi.org/10.1021/acs.jctc.1c00810.

[28] H.M. Berman, J. Westbrook, Z. Feng, G. Gilliland, T.N. Bhat, H. Weissig, I. N. Shindyalov, P.E. Bourne, The protein data bank, Nucleic Acids Res. 28 (2000) 235–242, https://doi.org/10.1093/nar/28.1.235.

[29] M. Varadi, S. Anyango, M. Deshpande, S. Nair, C. Natassia, G. Yordanova, D. Yuan, O. Stroe, G. Wood, A. Laydon, A. Žídek, T. Green, K. Tunyasuvunakool, S. Petersen, J. Jumper, E. Clancy, R. Green, A. Vora, M. Lutfi, M. Figurnov, A. Cowie, N. Hobbs, P. Kohli, G. Kleywegt, E. Birney, D. Hassabis, S. Velankar, AlphaFold Protein Structure Database: massively expanding the structural coverage of protein-sequence space with high-accuracy models, Nucleic Acids Res. 50 (D1) (2022) D439–D444, https://doi.org/10.1093/nar/gkab1061.

[30] X. Peng, X. Wang, W. Qi, R. Su, Z. He, Affinity of rosmarinic acid to human serum albumin and its effect on protein conformation stability, Food Chem. 192 (2016) 178–187, https://doi.org/10.1016/j.foodchem.2015.06.109.

[31] J. Liu, Y. Kong, J. Miao, X. Mei, S. Wu, Y. Yan, X. Cao, Spectroscopy and molecular docking analysis reveal structural specificity of flavonoids in the inhibition of α-glucosidase activity, Int. J. Biol. Macromol. 152 (2020) 981–989, https://doi.org/10.1016/j.ijbiomac.2019.10.184.

[32] H. Wu, W. Zeng, L. Chen, B. Yu, Y. Guo, G. Chen, Z. Liang, Integrated multi-spectroscopic and molecular docking techniques to probe the interaction mechanism between maltase and 1-deoxynojirimycin, an α-glucosidase inhibitor, Int. J. Biol. Macromol. 114 (2018) 1194–1202, https://doi.org/10.1016/j.ijbiomac.2018.04.024.

[33] W. Wang, Y. Yagiz, T.J. Buran, C. do Nascimento Nunes, L. Gu, Phytochemicals from berries and grapes inhibited the formation of advanced glycation end-products by scavenging reactive carbonyls, Food Res. Int. 44 (9) (2011) 2666–2673, https://doi.org/10.1016/j.foodres.2011.05.022.

[34] A.E. Maccarronello, N. Cardullo, A.M. Silva, A. Di Francesco, P.C. Costa, F. Rodrigues, V. Muccilli, Unlocking the nutraceutical potential of *Corylus avellana* L. shells: microwave-assisted extraction of phytochemicals with antiradical and anti-diabetic properties, J. Sci. Food Agric. 104 (15) (2024) 9472–9485, https://doi.org/10.1002/jsfa.13770.

[35] F.A. Qais, I. Ahmad, Mechanism of non-enzymatic antiglycation action by coumarin: a biophysical study, RSC New J. Chem. 43 (2019) 12823–12835, https://doi.org/10.1039/C9NJ01490J.

[36] A. Gupta, M. Khursheed, Z. Arif, A. Badar, K. Ala, Methylglyoxal-induces multiple stable changes in human serum albumin before forming nephrotoxic advanced glycation end-products: injury demonstration in human embryonic kidney cells, Int. J. Biol. Macromol. 214 (2022) 252–263, https://doi.org/10.1016/j.ijbiomac.2022.06.096.

[37] A. Ahmed, A. Shamsi, M.S. Khan, F.M. Husain, B. Bano, Methylglyoxal induced glycation and aggregation of human serum albumin: Biochemical and biophysical approach, Int. J. Biol. Macromol. 113 (2018) 269–276, https://doi.org/10.1016/j.ijbiomac.2018.02.137.

[38] R.L. Levine, D. Garland, C.N. Oliver, A. Amici, I. Climent, A.G. Lenz, B.W. Ahn, S. Shaltiel, E.R. Stadtman, Determination of carbonyl content in oxidatively modified proteins, Methods Enzymol. 186 (1990) 464–478, https://doi.org/10.1016/0076-6879(90)86141-H.

[39] A. Haque, M.W.A. Khan, K.M. Alenezi, R. Soury, M.S. Khan, S. Ahamad, M. Mushtaque, D. Gupta, Synthesis, characterization, antiglycation evaluation, molecular docking, and ADMET studies of 4-thiazolidinone derivatives, ACS Omega 9 (1) (2023) 1810–1820, https://doi.org/10.1021/acsomega.3c08463.

[40] M. Minekus, M. Alminger, P. Alvito, S. Ballance, T. Bohn, C. Bourlieu, F. Carrière, R. Boutrou, M. Corredig, D. Dupont, C. Dufour, L. Egger, M. Golding, S. Karakaya, B. Kirkhus, S. Le Feunteun, U. Lesmes, A. Macierzanka, A. Mackie, S. Marze, D. J. McClements, O. Ménard, I. Recio, C.N. Santos, R.P. Singh, G.E. Vegarud, M.S. J. Wickham, W. Weitschies, A. Brodkorb, A standardised static *in vitro* digestion method suitable for food - an international consensus, Food Funct. 5 (6) (2014) 1113–1124, https://doi.org/10.1039/c3fo60702j.

[41] A.E. Maccarronello, N. Cardullo, D. Pinto, A. Di Francesco, M.G.G. Pittalà, F. Rodrigues, V. Muccilli, Exploring the metabolic fate of antioxidant and hypoglycemic compounds from *Pistacia vera* shells through *in vitro* simulated digestion and untargeted metabolomics, Food Chem. 485 (2025) 144514, https://doi.org/10.1016/j.foodchem.2025.144514.

[42] N. Feng, Y. Feng, F. Zhang, J. Yan, M. Niu, L. Shi, H. Xiong, M. Zhou, Q. Wu, Inhibition mechanism of mango vinegar on protein-AGEs digestion *in vitro* gastrointestinal environment, LWT 186 (2023) 115246, https://doi.org/10.1016/j.lwt.2023.115246.

[43] K. Jones, L. Sim, S. Mohan, J. Kumarasamy, H. Liu, S. Avery, H.Y. Naim, R. Quezada-Calvillo, B.L. Nichols, B.M. Pinto, D.R. Rose, Mapping the intestinal alpha-glucogenic enzyme specificities of starch digesting maltase-glucoamylase and sucrase-isomaltase, Bioorg. Med. Chem. 19 (13) (2011) 3929–3934, https://doi.org/10.1016/j.bmc.2011.05.033.

[44] L. Sun, M. Miao, Dietary polyphenols modulate starch digestion and glycaemic level: a review, Crit. Rev. Food Sci. Nutr. 60 (4) (2020) 541–555, https://doi.org/10.1080/10408398.2018.1544883.

[45] S. Taj, M. Ahmad, U.A. Ashfaq, Exploring of novel 4-hydroxy-2H-benzo e 1,2 thiazine-3-carbohydrazide 1,1-dioxide derivative as a dual inhibitor of a-glucosidase and a-amylase: molecular docking, biochemical, enzyme kinetic and in-vivo mouse model study, Int. J. Biol. Macromol. 207 (2022) 507–521, https://doi.org/10.1016/j.ijbiomac.2022.03.023.

[46] T. Palmer, P.L. Bonner, 8 - enzyme inhibition, in: T. Palmer, P.L. Bonner (Eds.), Enzymes, Second edition, Woodhead Publishing, 2011, pp. 126–152.

[47] B.S. Dlamini, C. Chen, W. Shih, Y. Chen, J. Hsu, C. Chang, Insights into the α-amylase and α-glucosidase inhibition mechanism of 4-(4-hydroxyphenyl)-but-3-en-2-one from *Scutellaria barbata* D. Don: enzymatic kinetics, fluorescence spectroscopy and computational simulation, Med. Chem. Res. 31 (11) (2022) 2007–2020, https://doi.org/10.1007/s00044-022-02966-z.

[48] J. Liu, Y. Liu, X. He, B. Teng, J.M. McRae, Valonea tannin: tyrosinase inhibition activity, structural elucidation and insights into the inhibition mechanism, Molecules 26 (9) (2021) 2747, https://doi.org/10.3390/molecules26092747.

[49] J. Yan, G. Zhang, J. Pan, Y. Wang, α-Glucosidase inhibition by luteolin: kinetics, interaction and molecular docking, Int. J. Biol. Macromol. 64 (2014) 213–223, https://doi.org/10.1016/j.ijbiomac.2013.12.007.

[50] R. Gonçalves, N. Mateus, V. de Freitas, Inhibition of α-amylase activity by condensed tannins, Food Chem. 125 (2) (2011) 665–672, https://doi.org/10.1016/j.foodchem.2010.09.061.

[51] S. Quraishi, S. Nudrat, K. Kumari, E.W.M. Marboh, K. Aguan, A.S. Roy, Elucidation of inhibitory effects of bioactive anthraquinones towards formation of DNA advanced glycation end products (DNA-AGEs), Int. J. Biol. Macromol. 269 (2) (2024) 131810, https://doi.org/10.1016/j.ijbiomac.2024.131810.

[52] N. Cardullo, A.E. Maccarronello, B. Melilli, L. Vitiello, A.A. Scamporrino, A. M. Silva, C. Sciacca, A. Bacler, F. Rodrigues, V. Muccilli, Recovery of verbascoside from *Lantana camara* pruning waste for development of phytosomes with antioxidant and hypoglycemic properties, Ind. Crop. Prod. 236 (2025) 121829, https://doi.org/10.1016/j.indcrop.2025.121829.

[53] Q. Wu, S. Tang, L. Zhang, J. Xiao, Q. Luo, Y. Chen, M. Zhou, N. Feng, C. Wang, The inhibitory effect of the catechin structure on advanced glycation end product formation in alcoholic media, Food Funct. 11 (6) (2020) 5396–5408, https://doi.org/10.1039/C9FO02887K.

[54] J. Roy, D. Tiwari, S. Saha, R. Vankayala, S.S.R. Vuppaladadium, A. Joshi, I. Banerjee, Effect of bovine serum albumin (BSA) variants on the photophysical and biological properties of a NIR-responsive BSA-indocyanine green complex, Mater. Adv. 6 (2025) 1621–1634, https://doi.org/10.1039/D5MA00066A.

[55] A.R. Jyoti, S. Mir, S.S. Habib, A. Ali Siddiqui, Moinuddin., Neo-epitopes on methylglyoxal modified human serum albumin lead to aggressive autoimmune response in diabetes, Int. J. Biol. Macromol. 86 (2016) 799–809, https://doi.org/10.1016/j.ijbiomac.2016.02.019.

[56] T.A. Khan, M. Saleemuddin, A. Naeem, Partially folded glycated state of human serum albumin tends to aggregate, Int. J. Pept. Res. Ther. 17 (2011) 271, https://doi.org/10.1007/s10989-011-9267-7.

[57] Q. Li, K. Xiao, C. Yi, F. Yu, W. Wang, J. Rao, M. Liu, L. Zhang, Y. Mu, C. Wang, Q. Wu, D. Li, M. Zhou, Inhibition and mechanism of protein nonenzymatic glycation by *Lactobacillus fermentum*, Foods 13 (8) (2024) 1183, https://doi.org/10.3390/foods13081183.

[58] N. Chen, N. Wang, Q. Fang, Z. Yu, Y. Hu, J. Jin, S. Yang, Inhibition effect of AGEs formation *in vitro* by the two novel peptides EDYGA and DLLCIC derived from *Pelodiscus sinensis*, Front. Nutr. 12 (2025), https://doi.org/10.3389/fnut.2025.1537338.

[59] Q. Wu, Y. Ouyang, Y. Kong, Y. Min, J. Xiao, S. Li, M. Zhou, N. Feng, L. Zhang, Catechin inhibits the release of advanced glycation end products during glycated bovine serum albumin digestion and corresponding mechanisms in vitro, J. Agric. Food Chem. 69 (31) (2021) 8807–8818, https://doi.org/10.1021/acs.jafc.1c03348.